

***SMAI-JCM***  
SMAI JOURNAL OF  
COMPUTATIONAL MATHEMATICS

A combined first and second order  
model for a junction with ramp  
buffer

JENNIFER WEISSEN, OLIVER KOLB & SIMONE GÖTTLICH

Volume 8 (2022), p. 349-374.

<https://doi.org/10.5802/smai-jcm.90>

© The authors, 2022.



*The SMAI Journal of Computational Mathematics is a member  
of the Centre Mersenne for Open Scientific Publishing*

<http://www.centre-mersenne.org/>

Submissions at <https://smai-jcm.centre-mersenne.org/ojs/submission>

e-ISSN: 2426-8399



## A combined first and second order model for a junction with ramp buffer

JENNIFER WEISSEN<sup>1</sup>  
OLIVER KOLB<sup>2</sup>  
SIMONE GÖTTLICH<sup>3</sup>

<sup>1</sup> University of Mannheim, Department of Mathematics, 68131 Mannheim, Germany

*E-mail address:* jennifer.weissen@uni-mannheim.de

<sup>2</sup> University of Mannheim, Department of Mathematics, 68131 Mannheim, Germany

*E-mail address:* kolb@uni-mannheim.de

<sup>3</sup> University of Mannheim, Department of Mathematics, 68131 Mannheim, Germany

*E-mail address:* goettlich@uni-mannheim.de.

**Abstract.** Second order macroscopic traffic flow models are able to reproduce the so-called capacity drop effect, i.e., the phenomenon that the outflow of a congested region is substantially lower than the maximum achievable flow. Within this work, we propose a first order model for a junction with ramp buffer that is solely modified at the intersection so that the capacity drop is captured. Theoretical investigations motivate the new choice of coupling conditions and illustrate the difference to purely first and second order models. The numerical example considering the optimal control of the onramp merging into a main road highlights that the combined model generates similar results as the second order model.

**2020 Mathematics Subject Classification.** 65M08, 90C30.

**Keywords.** traffic flow, numerical analysis, ramp metering control.

### 1. Introduction

Starting with the pioneering works on the Lighthill–Whitham–Richards (LWR) model [36, 41], traffic flow models based on scalar conservation laws, i.e., macroscopic traffic models, have received considerable attention in the academic literature over the past decades. Macroscopic models are mainly distinguished in first order models, which consist of a scalar conservation law for the traffic density, and second order models, using a system of two conservation or balance laws with an additional equation for the mean traffic speed. The first order LWR model describes the time evolution of the traffic density  $\rho$ . The main drawback of the LWR model is the direct link of the velocity and flux to the traffic density, which does not allow for a correct description of traffic instabilities. Second order models have been developed aiming to improve traffic descriptions. Aw, Rascle and Zhang [4, 45] introduced the second order ARZ model which is capable to capture traffic instabilities and additionally overcame the drawbacks of earlier developed second order models, see [12]. They introduced a pressure function  $p(\rho)$  in the dynamics. The pressure function represents an anticipation factor, which takes into account the reaction of drivers to the traffic in front of them [18]. It defines the relation between the density  $\rho$  and the speed  $v$  in the fundamental diagram via a Lagrangian marker  $w$ . In comparison to the LWR model, the second order model enables to portray more important traffic phenomena [44]. Greenberg [21] extended the ARZ model with a relaxation term towards a preferred velocity. This extension in turn was further generalized by [42]. Since then, the extension to traffic flow on road networks has been investigated intensively, see for example [7, 10, 17, 19, 20, 23, 27, 28, 31]. The

---

This work was supported by the DFG grant No. GO 1920/7-1 and by DAAD (Project-ID 57445223).

<https://doi.org/10.5802/smai-jcm.90>

© The authors, 2022

crucial point at intersections is the definition of suitable coupling conditions, i.e., conservation of mass and possibly momentum in the case of second order models.

Many interesting effects within traffic dynamics related to congestion and traffic jams have been investigated for microscopic, mesoscopic and macroscopic traffic models, see [25]. Among these effects, the so-called capacity drop phenomenon is of interest [20, 23, 24, 34, 38]. The capacity drop is the phenomenon that the outflow of a congested region is significantly lower than the maximum achievable flow in this region. A capacity drop is observed when the traffic volume upstream of a bottleneck increases, but the discharge flow leaving the bottleneck decreases in comparison to the flow measured prior to the increase in traffic volume [9]. Studies conducted on freeways showed that the discharge flow diminishes with the onset of upstream queues [5, 8, 22]. This results in a flow lower than the maximum one. The traffic jams arising from the capacity drop at bottlenecks can even become permanent [24].

Specifically, in case of an onramp at a freeway, the capacity drop is explained by the fact that drivers mutually impede each other, when too many vehicles try to access the main road [38]. Additionally, drivers at the incoming road upstream from the onramp entry are impacted and might break and slow down. While vehicles can decelerate fast, the acceleration process takes substantially longer [35].

The capacity drop has major influence on the traffic flow and is especially important in the consideration of traffic control. In general, the observational findings indicate that approaches to control the traffic density are promising for increasing bottleneck discharge flows [9].

Here, we completely stick to the LWR model to describe the dynamics on the roads. To mirror the capacity drop effect, we put special emphasis on the intersections, where the velocities and Lagrangian markers are incorporated to describe the dynamics. The capacity drop is achieved by a flow reduction derived from second order dynamics rather than by an adaption of the fundamental diagram. We therefore consider a first order macroscopic model on the roads and we merely apply adapted coupling conditions of a second order macroscopic model at the junctions. This combination then allows to model the capacity drop effect.

A similar approach has been considered in [26], where the LWR model was coupled to a kinetic model at the junctions. Comparable to [26], the combined model is also able to cover the capacity drop phenomenon. As in [13], our model is a first order model with a point constraint at the junction. In both models, the supply function of the outgoing road incorporates information of the upstream traffic conditions. The junction constraint in this work is motivated by the second order ARZ model and combines the first order approach with some second order information. Using the combined model, we apply a discrete optimization approach for the control of the onramp, see e.g. [19, 20, 40]. The combined model serves as a suitable substitute model for a second order model when investigating optimal control strategies for ramp metering.

The paper is organized as follows: In Section 2, we briefly recall the LWR and ARZ model. Section 3.1 discusses the capacity drop. We construct our combined model in Section 3.2 with specific emphasis on the respective demand and supply functions, which determine the flux at the junction. The supply function is analyzed intensively in Section 3.3. In Section 4, we present a numerical comparison for several Riemann problems in the LWR and the combined model based on the discretization in Section 4.1 and Section 4.2. The ability to capture the capacity drop is illustrated in Table 4.1. Section 4.3 presents a comparison of the combined model with second order models. The numerical discretization for second order models is introduced in Section 4.3.1 and comparisons of the combined model with second order models are drawn in Section 4.3.2. The paper concludes with numerical results for an optimal control problem for ramp metering in Section 4.3.3.

## 2. Models and notations for traffic flow

We consider a directed graph  $G = (\mathcal{V}, \mathcal{E})$  with a finite number of roads  $e \in E$  and junctions  $k \in \mathcal{V}$ . The roads  $e$  are modeled by intervals  $(a_e, b_e)$  with (possibly infinite) lengths  $L_e = b_e - a_e$ . Vehicles are treated as a continuum with density  $\rho$  and velocity  $v$ . We shortly introduce two well-known first and second order macroscopic approaches for traffic flow on networks and explain how they model a junction with ramp buffer.

### 2.1. The LWR model

Given an initial density  $\rho_e(x, 0)$  and denoting  $\rho_e = \rho_e(x, t)$ , the dynamics of the LWR model are given by

$$\partial_t \rho_e + \partial_x (\rho_e V(\rho_e)) = 0, \quad (x, t) \in (a_e, b_e) \times \mathbb{R}_{\geq 0}, \quad (2.1)$$

on each road  $e$ . Here, we choose for each road  $e$  the linear velocity function

$$V(\rho_e) = v^{\max} \left( 1 - \frac{\rho_e}{\rho^{\max}} \right), \quad (2.2)$$

with maximum velocity  $v^{\max}$  and maximum density  $\rho^{\max}$  as for example described in [17]. We denote the concave flux function  $f(\rho_e) = \rho_e V(\rho_e)$ . It holds that  $f(0) = f(\rho^{\max}) = 0$  and the density  $\rho^{\max}/2$  maximizes the flux in the interval  $[0, \rho^{\max}]$ . Traffic flow  $f$  and velocity  $V$  are directly coupled to the traffic density  $\rho$ .

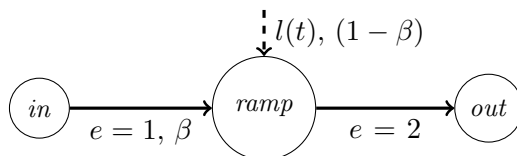


FIGURE 2.1. 1-to-1 junction with an onramp.

In this work, we are especially interested in the dynamics at a junction with ramp buffer. Figure 2.1 illustrates the 1-to-1 junction with an onramp at the node *ramp*, which is examined in the following. For simplicity, we assume as prescribed in (2.1) that the roads  $e = 1, 2$  have the same parameters  $\rho^{\max}$ ,  $v^{\max}$ . At the onramp traffic is allowed to enter the outgoing road  $e = 2$  and the parameter  $\beta$  describes the mixture of incoming traffic from road  $e = 1$  and from the onramp. The quantity  $l(t)$  describes the length of the queue at the ramp buffer and is modeled by the following ordinary differential equation (ODE):

$$\frac{dl(t)}{dt} = f_{\text{or}}^{\text{in}}(t) - q_{\text{or}}(t), \quad t \in \mathbb{R}_{\geq 0}, \quad (2.3)$$

where  $f_{\text{or}}^{\text{in}}$  denotes a (possibly) time-dependent flux that enters the onramp from outside of the network and  $q_{\text{or}}$  is the flux that exits from the onramp to the outgoing road  $e = 2$ .

To define an initial value problem for this particular network structure, we consider Riemann data on the incoming and outgoing road, i.e.,  $\rho_e(x, 0) = \rho_e^0$ ,  $e = 1, 2$  and a fixed inflow  $f_{\text{or}}^{\text{in}} > 0$  from the onramp. The end of the incoming road is set to  $b_1 = 0$  and the beginning of the outgoing road to  $a_2 = 0$ , such that the junction is located at  $x = 0$ . Then, the (half-) Riemann problem for the roads

and the evolution of the queue length at the junction reads

$$\begin{cases} \partial_t \rho_e + \partial_x (\rho_e V(\rho_e)) = 0, & (x, t) \in (a_e, b_e) \times \mathbb{R}_{\geq 0}, \quad e = 1, 2, \\ \rho_e(x, 0) = \begin{cases} \rho_e^+ & \text{for } x > 0 \\ \rho_e^- & \text{for } x \leq 0, \end{cases} & x \in (a_e, b_e), \quad e = 1, 2, \\ \frac{dl(t)}{dt} = f_{\text{or}}^{\text{in}} - q_{\text{or}}(t), & t \in \mathbb{R}_{\geq 0}, \\ l(0) = l^0. \end{cases} \quad (2.4)$$

Here,  $l^0 \geq 0$  indicates the initial buffer load. Depending on whether the road is incoming or outgoing, only one of the Riemann data  $\rho_e^-, \rho_e^+$  is defined for  $t = 0$ . In particular, for road  $e = 1$  entering the junction  $\rho_1^- = \rho_1^0$ , and for the road  $e = 2$  exiting the junction  $\rho_2^+ = \rho_2^0$ . The other datum as well as the flux  $q_{\text{or}}(t)$  exiting the onramp is defined by the solution through some suitable coupling conditions at the junction. This will be the focus of this work. We fix a priority parameter  $\beta$  and define the mixture rule:

**(M1).** In case that not all cars can enter the outgoing road, let  $q$  be the flux that can enter the outgoing road. Then  $\beta q$  comes from the incoming road  $e = 1$  and  $(1 - \beta)q$  comes from the onramp. In case that the amounts  $\beta q$  (resp.  $(1 - \beta)q$ ) cannot be served from the incoming road (resp. onramp), we allow that the missing amount is filled up by the onramp (resp. incoming road).

We define solutions to (2.4) in the following, compare also [14].

**Definition 2.1.** A triple  $(\rho_1, \rho_2, l)$  is called an admissible weak solution to (2.4) if the following holds:

- The densities  $\rho_e : (a_e, b_e) \times [0, \infty) \rightarrow [0, \rho^{\text{max}}]$ ,  $e = 1, 2$  are weak solutions such that

$$\int_0^\infty \int_{a_e}^{b_e} (\rho_e \partial_t \phi_e + f(\rho_e) \partial_x \phi_e) dx dt = 0, \quad e = 1, 2,$$

for every test function  $\phi_e : (a_e, b_e) \times \mathbb{R}_{\geq 0} \rightarrow \mathbb{R}$  with compact support.

- The densities  $\rho_e$ ,  $e = 1, 2$  satisfy the Kruzhkov entropy condition [32]. I.e., for  $z \in \mathbb{R}$  and  $\phi_e : (a_e, b_e) \times \mathbb{R}_{\geq 0} \rightarrow \mathbb{R}$  smooth, positive with compact support, we have that

$$\int_0^\infty \int_{a_e}^{b_e} (|\rho_e - z| \partial_t \phi_e + \text{sign}(\rho_e - z) (f(\rho_e) - f(z)) \partial_x \phi_e) dx dt + \int_{a_e}^{b_e} |\rho_e^0 - z| \phi_e(x, 0) dx \geq 0, \quad e = 1, 2. \quad (2.5)$$

- The conservation of mass at the junction is fulfilled

$$\underbrace{f(\rho_1(0, t))}_{:=q_1} + q_{\text{or}}(t) = \underbrace{f(\rho_2(0, t))}_{:=q_2}.$$

- The flux entering the outgoing road is maximal subject to the mixture rule (M1).
- The queue length  $l$  is a solution of (2.3) for almost every  $t \in \mathbb{R}_{\geq 0}$ .

Let  $q_1, q_{\text{or}}$  denote the initially unknown mass flux coming from the incoming road and the onramp. The total flux has to exit into the outgoing road such that  $q_2 = q_1 + q_{\text{or}}$ . In agreement with the literature [10, 34], we employ the widely used demand and supply formulation for admissible flux values. The fluxes at the junction are bounded by demand and supply

$$0 \leq q_1 \leq D^{\text{LWR}}(\rho_1), \quad 0 \leq q_{\text{or}} \leq D^{\text{or}}(l), \quad 0 \leq q_2 \leq S^{\text{LWR}}(\rho_2).$$

These are used to determine the flux at the junction and allow for an appropriate description of the coupling and boundary conditions [34]. The demand  $D^{\text{LWR}}(\rho_1)$  of the incoming road and the supply  $S^{\text{LWR}}(\rho_2)$  of the outgoing road are defined as follows:

$$D^{\text{LWR}}(\rho_1) = \begin{cases} \rho_1 V(\rho_1) & \text{if } \rho_1 \leq \frac{\rho^{\max}}{2}, \\ f^{\max} & \text{if } \rho_1 > \frac{\rho^{\max}}{2}, \end{cases} \quad S^{\text{LWR}}(\rho_2) = \begin{cases} f^{\max} & \text{if } \rho_2 \leq \frac{\rho^{\max}}{2}, \\ \rho_2 V(\rho_2) & \text{if } \rho_2 > \frac{\rho^{\max}}{2}, \end{cases} \quad (2.6)$$

where  $f^{\max} = f(\rho^{\max}/2)$ . Moreover, the demand of the onramp is modeled by

$$D^{\text{or}}(l) = \begin{cases} f_{\text{or}}^{\max} & \text{if } l > 0, \\ \min\{f_{\text{or}}^{\text{in}}(t), f_{\text{or}}^{\max}\} & \text{otherwise,} \end{cases} \quad (2.7)$$

where  $f_{\text{or}}^{\max}$  denotes the maximum flux which is allowed to enter from the onramp into the outgoing road, i.e., a physical restriction on the number of cars per time unit that can exit from the onramp. Collecting together equations (2.6)–(2.7) and the mixture rule (M1), we can formulate the mass fluxes at the 1-to-1 junction with onramp according to the reference [19] in the compact form

$$\begin{aligned} q_1 &= \min\{D^{\text{LWR}}(\rho_1), \max\{\beta S^{\text{LWR}}(\rho_2), S^{\text{LWR}}(\rho_2) - D^{\text{or}}(l)\}\}, \\ q_{\text{or}} &= \min\{D^{\text{or}}(l), \max\{(1 - \beta)S^{\text{LWR}}(\rho_2), S^{\text{LWR}}(\rho_2) - D^{\text{LWR}}(\rho_1)\}\}, \\ q_2 &= q_1 + q_{\text{or}}, \end{aligned}$$

The above expression clarifies that the fluxes at the junction are obtained from the densities on incoming and outgoing road as well as the queue length at the onramp. It is a first order approach where velocity and flux at the junction are directly linked to the traffic densities  $\rho_1, \rho_2$ . The demand is obtained purely from the density on the incoming road  $\rho_1$  and the supply purely from the density on the outgoing road  $\rho_2$ . All in all, it is a simple and robust model to describe traffic flow [34]. Although the LWR model can predict some traffic situations rather well, the model exhibits various deficits [12]. In general, the model cannot portray traffic instabilities, which include growing traffic waves and so-called capacity drops [44].

## 2.2. The ARZ and the Greenberg model

In the second order ARZ model, the traffic density  $\rho_e = \rho_e(x, t)$  and velocity  $v_e = v_e(x, t)$  are not directly coupled, but evolve according to a system of conservation laws

$$\partial_t \begin{pmatrix} \rho_e \\ \rho_e w_e \end{pmatrix} + \partial_x \begin{pmatrix} \rho_e v_e \\ \rho_e v_e w_e \end{pmatrix} = 0, \quad (x, t) \in (a_e, b_e) \times \mathbb{R}_{\geq 0}. \quad (2.8)$$

The first equation describes the conservation of mass and the second equation includes the evolution of the vehicle speed. The Lagrangian marker  $w_e$  for each road in (2.8) is defined by the relation

$$w_e = v_e + p(\rho_e), \quad (2.9)$$

where we assume for simplicity that the pressure function  $p(\rho_e)$  is identical on all roads. The ARZ model is hyperbolic with eigenvalues  $\lambda_1 = v_e - \rho_e p'(\rho_e) \leq \lambda_2 = v_e$  and Riemann invariants  $w_e$  and  $v_e$ , see [4]. In this case, the Lagrangian marker  $w_e$  travels with the velocity  $v_e$  of the cars. It can be seen as a driver attribute describing the empty road velocity of drivers.

The pressure function  $p(\rho_e) \sim \rho_e^\gamma$  with  $\gamma = 2$  is the prototype function in traffic flow [4, 16] from which the Lagrangian marker (2.9) is computed. Here, we consider the pressure function from [20, 23, 38] given by

$$p(\rho_e) = \frac{v^{\max}}{2} \left( \frac{\rho_e}{\rho^{\max}} \right)^2, \quad (2.10)$$

which was derived from microscopic considerations [3]. The pressure function satisfies  $p'(\rho_e) > 0$  and  $\rho_e p''(\rho_e) + 2p'(\rho_e) > 0$  for all  $\rho_e$ . The former property ensures that the pressure function is

strictly increasing and the latter ensures the existence of a point  $\sigma(w_e)$  that maximizes the flux  $\rho_e v_e = \rho_e(w_e - p(\rho_e))$  for a given value of  $w_e$ . The inverse function of the pressure function is given by

$$p^{-1}(y) = \rho^{\max} \left( \frac{2y}{v^{\max}} \right)^{\frac{1}{2}}, \quad (2.11)$$

and  $\sigma(w_e)$  can also be computed explicitly

$$\sigma(w_e) = \operatorname{argmax}_{\rho_e \in [0, \rho^{\max}]} \rho_e(w_e - p(\rho_e)) = \rho^{\max} \left( \frac{2w_e}{3v^{\max}} \right)^{\frac{1}{2}}. \quad (2.12)$$

The (half-)Riemann problem for the ARZ model at the 1-to-1 junction with onramp located at  $x = 0$  reads:

$$\begin{cases} \partial_t \begin{pmatrix} \rho_e \\ \rho_e w_e \end{pmatrix} + \partial_x \begin{pmatrix} \rho_e v_e \\ \rho_e w_e v_e \end{pmatrix} = 0, & (x, t) \in (a_e, b_e) \times \mathbb{R}_{\geq 0}, e = 1, 2, \\ (\rho_e, w_e)(x, 0) = \begin{cases} (\rho_e^+, w_e^+) & \text{for } x > 0 \\ (\rho_e^-, w_e^-) & \text{for } x \leq 0, \end{cases} & x \in (a_e, b_e), e = 1, 2, \\ \frac{dl(t)}{dt} = f_{\text{or}}^{\text{in}} - q_{\text{or}}(t), & t \in \mathbb{R}_{\geq 0}, \\ l(0) = l^0. \end{cases} \quad (2.13)$$

As for the first order model, we formulate the admissible fluxes at the junction through a demand and supply framework. Following [20, 28], the demand and supply functions for the ARZ model are given by

$$D^{\text{ARZ}}(\rho, w) = \begin{cases} \rho(w - p(\rho)) & \text{if } \rho \leq \sigma(w), \\ \sigma(w)(w - p(\sigma(w))) & \text{if } \rho > \sigma(w), \end{cases} \quad (2.14)$$

$$S^{\text{ARZ}}(\rho, w) = \begin{cases} \sigma(w)(w - p(\sigma(w))) & \text{if } \rho \leq \sigma(w), \\ \rho(w - p(\rho)) & \text{if } \rho > \sigma(w). \end{cases} \quad (2.15)$$

Without entering the discussion in detail, by knowledge on the Riemann solution of the hyperbolic second order model, see e.g. [6, 33], we know that the Riemann problem for (2.8) on the whole line  $x \in \mathbb{R}$  with traffic state  $U_L = (\rho_L, \rho_L w_L)$  on the left ( $x \leq 0$ ) and  $U_R = (\rho_R, \rho_R w_R)$  on the right ( $x > 0$ ), is solved by a 1-wave connecting  $U_L, \tilde{U}$  and a 2-contact-discontinuity connecting  $\tilde{U}, U_R$ , see also [4]. The intermediate state is given by  $\tilde{U} = (\tilde{\rho}, \tilde{\rho} w_L)$  and satisfies  $v(\tilde{U}) = v_R$ , i.e., the second order velocity is given by the velocity of the density on the right.

This can be transferred to define solutions to the (half-) Riemann problem in (2.13). We follow the approach of [20] to define the Riemann solver at the 1-to-1 junction with onramp: We choose to rewrite the supply function (2.15) at the 1-to-1 junction with onramp depending on the traffic states left and right from the junction

$$S^{\text{ARZ}}(\rho_1, \rho_2, w_1, v_2) = \begin{cases} \sigma(w_1)(w_1 - p(\sigma(w_1))) & \text{if } \tilde{\rho} \leq \sigma(w_1), \\ \tilde{\rho}(w_1 - p(\tilde{\rho})) & \text{if } \tilde{\rho} > \sigma(w_1). \end{cases} \quad (2.16)$$

The mass flux at the interface  $x = 0$  is determined by the intermediate density value  $\tilde{\rho}$  where  $\tilde{\rho} = \tilde{\rho}(\rho_1, \rho_2, w_1, v_2)$  is the density of the state  $\tilde{U}$  such that  $w(\tilde{U}) = v_1 + p(\rho_1)$  and  $v(\tilde{U}) = v_2$ . By assumption on the pressure function, there exists at most one state with  $\tilde{\rho} \neq 0$  satisfying these conditions<sup>1</sup>. The

<sup>1</sup>We remark that the approach in [20] works with a fixed pressure function  $p$ . There are also Riemann solvers considering a change in the pressure function after merge type junctions [27, 28].

mass fluxes for the 1-to-1 junction with onramp according to [20] are then given by

$$\begin{aligned} q_1 &= \min \left\{ D^{\text{ARZ}}(\rho_1, w_1), \max \left\{ \beta S^{\text{ARZ}}, S^{\text{ARZ}} - D^{\text{or}}(l) \right\} \right\}, \\ q_{\text{or}} &= \min \left\{ D^{\text{or}}(l), \max \left\{ (1 - \beta) S^{\text{ARZ}}, S^{\text{ARZ}} - D^{\text{ARZ}}(\rho_1, w_1) \right\} \right\}, \\ q_2 &= q_1 + q_{\text{or}}, \end{aligned} \tag{2.17}$$

where  $S^{\text{ARZ}} = S^{\text{ARZ}}(\rho_1, \rho_2, w_1, v_2)$ . One weakness of the ARZ model as pointed out e.g. by Greenberg [21] is that drivers travelling at speed  $v_e$  in traffic with local density  $\rho_e$  never try to adjust their speed to a maximum allowable speed  $V(\rho_e)$ . The ARZ model might be extended with a relaxation term on the right-hand side of the second equation to correct this weakness, see e.g. [3, 4, 21]. Given initial densities and velocities, the traffic dynamics are governed by the equations

$$\partial_t \begin{pmatrix} \rho_e \\ \rho_e w_e \end{pmatrix} + \partial_x \begin{pmatrix} \rho_e v_e \\ \rho_e w_e v_e \end{pmatrix} = \begin{pmatrix} 0 \\ -\rho_e \frac{v_e - V(\rho_e)}{\tau} \end{pmatrix}, \quad (x, t) \in (a_e, b_e) \times \mathbb{R}_{\geq 0}. \tag{2.18}$$

The relaxation term on the right-hand side includes that drivers tend to adopt an equilibrium (or preferential) speed  $V(\rho_e)$ . The factor  $\tau > 0$  is interpreted as relaxation time towards an equilibrium speed  $V(\rho_e)$ . In the numerical examples, we use the model (2.18) with the LWR velocity given by (2.2) as equilibrium velocity. The model therefore possibly contains a relaxation towards the LWR model. For  $\tau = \infty$ , we obtain the original ARZ model. For any value  $\tau \in (0, \infty)$ , we obtain the relaxed model to which we will refer to as ‘‘Greenberg model’’ for simplicity in the following. The Greenberg model was mathematically derived from car following models in [3]. A generalization with a more flexible source term where the relaxation depends on the density and velocity is considered in [42, 43]. For an analytical convergence analysis of the Greenberg model for  $\tau \rightarrow 0$ , we refer to [3, 39]. Moreover, some numerical experiments comparing the Greenberg model with the LWR model are discussed in [20].

**Remark 2.2.** The source term in the Greenberg model (2.18) is relevant for the road dynamics but is neglected when considering Riemann problems at intersections [43]. Coupling conditions for the Greenberg model and the 1-to-1 junction with ramp buffer are therefore also given by (2.17).

### 3. Capacity drop and introduction of the combined model

First, we introduce the capacity drop. Then, we establish a new modeling approach, which combines first and second order traffic models at junction points leading to new coupling conditions.

#### 3.1. The capacity drop

Several traffic network models which equip the first order LWR model with coupling conditions at the junction [10, 29, 30] do not reproduce the capacity drop, see also the discussion in [24]. Lebacque [34] introduced an additional new state variable for the junction in the LWR model. Using this modification, the model is able to represent the capacity drop. Haut et al. [24] triggered a capacity drop by considering a  $\bar{g}$ -capacity drop function  $\bar{g}(\mathcal{Z})$  at the junction. If the sum of incoming demands  $\mathcal{Z}$  is above the maximum flux  $f^{\text{max}}$  of the outgoing road, the discharge flow at the junction is reduced. The shape of the flow reduction is prescribed by the  $\bar{g}$ -capacity drop function. Nonlocal point constraints limiting the discharging flow at the junction by averaging the density conditions upstream are considered in [1]. The constraint function at the junction  $x = 0$  depends on the solution itself in an upstream neighborhood  $x < 0$ . They analyzed the capacity drop in the model and further extended the nonlocal point constraint to the ARZ model [2].



Within the second order traffic network models, the capacity drop is included more naturally. The junction model by Haut and Bastin [23] is able to reproduce the capacity drop without the introduction of any new parameters compared to those of the single road model (2.8). Parzani and Buisson [38] study the model from [23] in a traffic scenario where the bottleneck is caused by an onramp. Furthermore, the Riemann solver in [20] for the junction with onramp, which we recalled in Section 2, shows that the Greenberg model is able to portray the capacity drop and can be applied within traffic control strategies.

In general, traffic control strategies aim to reduce the total time drivers spend in a traffic network. Drivers enter highways at onramps on several locations and controlling these entry points by ramp metering approaches can decrease the total travel time in comparison to the uncontrolled case [5]. For example, a control strategy for ramp metering that can manage to sustain high flows at the sources of the network leads to a decrease of the total time spent in the network [37]. A model covering the capacity drop is therefore an essential requirement for the development of traffic control strategies.

### 3.2. Construction of the combined model

We begin to develop a junction model for the 1-to-1 junction with ramp buffer covering the capacity drop. The junction model (2.17) of the Greenberg model includes the capacity drop, see [31]. However considering the second order dynamics, it comes at increased computational cost in comparison to the LWR model. The sharp analysis of second order models by Daganzo [12] states that the traffic for low densities is free and similar to the dynamics of the LWR model. We therefore represent the traffic on the incoming and outgoing road by the LWR model, which gives a good description for low densities. Our idea is now to customize the coupling conditions of the LWR model in case of increasing densities upstream of the junction. We denote the new model as augmented LWR model, or shortly ALWR.

By including second order quantities, we seek to achieve a capacity drop similar to the second order models. However, the velocity  $V_e = V(\rho_e)$  stays coupled to the density  $\rho_e$  and the derived  $w$ -value for each road is always given by  $w(\rho_e) = p(\rho_e) + V_e$  and thus, also coupled to the density. At the junction point, our coupling conditions do not only consider the actual density  $\rho_2$ , but additionally the velocity  $V_2$  and the upstream  $w$ -value  $w_1 = w(\rho_1)$ . The upstream  $w$ -value induces a nonlocal point constraint, similar to [13] at the junction point, manipulating the flow through the junction such that a capacity drop is achieved. As explained above, our coupling conditions are motivated by the second order coupling conditions for the ARZ model and we combine them with the standard LWR coupling conditions by means of the augmented supply function

$$S^{\text{ALWR}}(\rho_1, \rho_2, l) = \begin{cases} S^{\text{LWR}}(\rho_2) & \text{if } 0 \leq D^{\text{LWR}}(\rho_1) + D^{\text{or}}(l) \leq f^{\text{max}}, \\ \min\{S^{\text{LWR}}(\rho_2), S^{\text{ARZ}}(\rho_1, \rho_2, w_1, V_2)\} & \text{otherwise.} \end{cases} \quad (3.1)$$

To determine the demands, the LWR demand function (2.6) and the onramp demand (2.7) is applied. The value  $\mathcal{Z} = D^{\text{LWR}}(\rho_1) + D^{\text{or}}(l)$  indicates the cumulated desired inflow into the outgoing road. It was observed in experiments that the threshold of traffic density at which a capacity drop is observed is merely constant across the observation days [9]. When the demand is at the level of the road capacity, breakdown and congestion occur [38]. Therefore, the exceedance of the road capacity  $f^{\text{max}}$  in (3.1) is meant to trigger the formation of a jam upstream the junction.

Analogously to [24], the flux value  $\mathcal{Z}$  works as a switch that activates a reduction of the flow through the junction. Contrary to their approach, the reduction of the flow here does not only consider the level of the accumulated demand  $\mathcal{Z}$ , but also the interplay of (derived) traffic states up- and downstream the junction in  $S^{\text{ARZ}}$  using (2.16). In comparison with [1], the nonlocality is restricted only to the junction interface  $x = 0-$ .

In case that the cumulated desired inflow does not exceed the maximum flow  $f^{\text{max}}$  of the outgoing road, the supply function of the LWR model is applied. In contrast, to evaluate the supply at a junction

when the desired inflow exceeds the maximum flow, the minimum of the LWR and ARZ supply is used. Meaning that the incoming flow drops below the inflow predicted by the LWR model, if the application of the ARZ model to the situation with derived second order quantity  $w_1$  would lead to a lower inflow. In case of a flow reduction in comparison to the LWR model, we determine the flow by the ARZ supply (2.16) using the derived quantities  $w_1$  and  $V_2$  in the augmented supply function. For the coupling conditions using the augmented supply function, we introduce a quite useful partition of the phase plane, which we will explain in detail in the following.

### 3.3. Discussion of the augmented supply function

This section focuses on the investigation of the supply function in the combined model to show that the ALWR model reduces the flux at the junction in case of congestion. We analyze the problem (2.4) and examine the augmented supply function (3.1) in case that the desired inflow  $\mathcal{Z}$  exceeds the capacity of the outgoing road  $f^{\max}$ .

Using the LWR velocity (2.2) and the pressure function (2.10), the derived  $w$ -value reads

$$w(\rho_e) = V(\rho_e) + p(\rho_e) = v^{\max} \left( 1 - \frac{\rho_e}{\rho^{\max}} \right) + \frac{v^{\max}}{2} \left( \frac{\rho_e}{\rho^{\max}} \right)^2, \quad (3.2)$$

and is plotted along with the velocity function in Figure 3.1a.

To shorten the notation, we define the derived ARZ supply by

$$S^{\text{ARZ}}(\rho_1, \rho_2) = S^{\text{ARZ}}(\rho_1, \rho_2, w_1, V_2) = \begin{cases} \sigma_1(w_1 - p(\sigma_1)) & \text{if } \tilde{\rho} \leq \sigma_1, \\ \tilde{\rho}(w_1 - p(\tilde{\rho})) & \text{otherwise,} \end{cases} \quad (3.3)$$

in the analysis below. Here,  $\sigma_1 = \sigma(w(\rho_1))$  is the sonic point given by (2.12). Note that we are able to do this because we assume that the dynamics on the roads are described by the LWR model.

The value  $w_1$  scales the supply function and also determines the position of the sonic point  $\sigma_1$ . If we interpret the term  $(w_1 - p(\rho_1))$  as the velocity function, then  $w_1$  is the empty road velocity. In the ARZ model,  $w_1$  is a driver attribute describing the empty road velocity of different drivers and travels with the speed of car. In the LWR model, the empty road velocity is  $v^{\max}$ , which is prescribed by the velocity function (2.2) and identical for all drivers. Using the derived marker  $w_1$  in (3.3) can be seen as a correction to the empty road velocity depending on the density. For  $\rho = 0$ , we obtain  $w(0) = v^{\max}$ . For  $\rho = \rho^{\max}$ , we obtain  $w(\rho^{\max}) = v^{\max}/2$  with the specific choices (2.2) and (2.10), see also Figure 3.1a. The higher the density, the lower the maximum speed, drivers can reach. Since a reduction in  $w_1$  reduces the flux, we can understand the above correction in the  $w$ -value as a flux reduction for high density values, see Figure 3.1b. The value  $\tilde{\rho}$  in (3.3) determines the flux at the junction in the second order model. This intermediate density, which is used to evaluate the supply, is derived from the combination of  $\rho_1$  and  $\rho_2$ . Greenberg [21] refers to this property as the anticipatory nature of the ARZ model, i.e., that the density  $\rho$  and velocity  $v$  behind a contact are also determined by  $\rho, v$  ahead of it. Traditionally, in the coupling at the junction of the LWR model, no connection is made between the states of the incoming and outgoing road in the supply. We therefore introduced  $\tilde{\rho}$  motivated from the second order model to combine information from both roads in the supply. Here, the derived value of  $\tilde{\rho}$  decides which branch of the supply function (3.3) is used to evaluate the flux at the junction. It holds that  $\tilde{\rho}$  is either the intersection of the curves  $\{w(U) = w_1\}$  and  $\{v(U) = V_2\}$  or  $\tilde{\rho} = 0$ , see [4]. We can express  $\tilde{\rho}$  explicitly by

$$\tilde{\rho} = p^{-1}(\max\{w_1 - V_2, 0\}), \quad \text{where } w_1 = V_1 + p(\rho_1). \quad (3.4)$$

If we plug  $\tilde{\rho}$  in the augmented supply function (3.1), then the augmented supply can either take the value of the LWR supply or the derived ARZ supply. In situations where the LWR supply is lower than the derived ARZ supply, the ALWR model is equal to the LWR model in its description of traffic

dynamics. On the other hand, in situations where the derived ARZ supply is lower than the LWR supply, traffic flow at the junction is reduced and the model differs from the LWR model. Note that we aim to approximate the fluxes at the junction in the ARZ model, but not the traffic state or the solution structure since we keep the LWR model on the roads and only approximate the flux at the junction point.

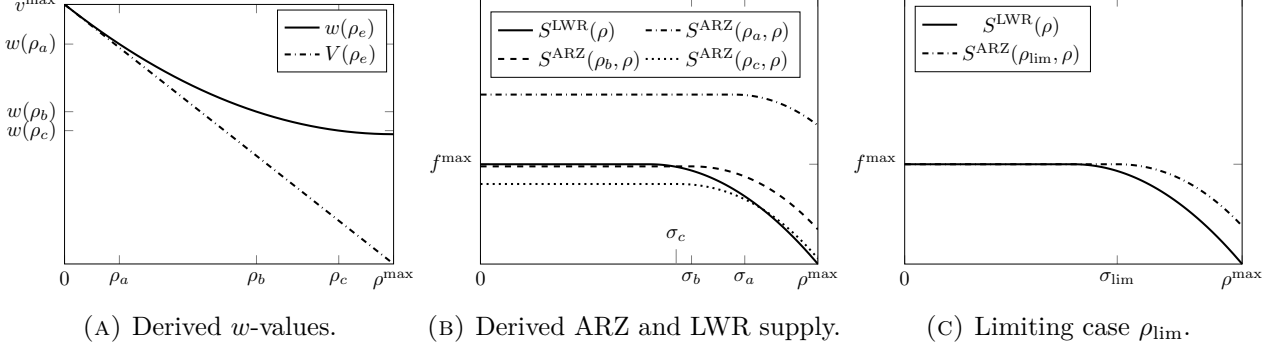


FIGURE 3.1. Supply functions

With  $\rho_{\text{lim}}$ , we denote the density for which we have

$$S^{\text{ARZ}}(\rho_{\text{lim}}, 0) = f^{\text{max}}, \quad (3.5)$$

see Figure 3.1c. This is used, among other criteria, to distinguish whether the ARZ or LWR supply is applied. The  $w$ -value is denoted  $w_{\text{lim}} = w(\rho_{\text{lim}})$ . Moreover, we observe from the combination of Figure 3.1a and Figure 3.1b that the supply functions are monotone decreasing with respect to the first as well as to the second argument. Plugging the densities  $\rho_1, \rho_2$  at the junction into the augmented supply function, we can distinguish the following cases:

**Case 1.** The LWR supply  $S^{\text{LWR}}(\rho_2)$  exceeds the maximum of the ARZ supply, which is exemplarily depicted in Figure 3.2a. The maximum of the ARZ supply (3.3) is

$$\max_{\rho_2 \in [0, \rho^{\text{max}}]} S^{\text{ARZ}}(\rho_1, \rho_2) = S^{\text{ARZ}}(\rho_1, 0),$$

for which  $\tilde{\rho} = 0$  since  $w_1 \leq v^{\text{max}}$ . The exceedance is only possible for  $\rho_1 \geq \rho_{\text{lim}}$ . In this case, the considered supply is the supply value from the ARZ model. This result is independent of the value  $\tilde{\rho}$ :

$$S^{\text{LWR}}(\rho_2) > S^{\text{ARZ}}(\rho_1, 0) \quad \Rightarrow \quad \min\{S^{\text{LWR}}(\rho_2), S^{\text{ARZ}}(\rho_1, \rho_2)\} = S^{\text{ARZ}}(\rho_1, \rho_2).$$

**Case 2.** The LWR supply for  $\rho_2$  exceeds the ARZ supply for some values, but it is below the maximum of the ARZ supply,

$$S^{\text{LWR}}(\rho_2) \leq S^{\text{ARZ}}(\rho_1, 0),$$

Then, one has to distinguish further depending on  $\tilde{\rho}$ :

(a). The ARZ supply evaluated at  $\tilde{\rho}$  exceeds the LWR supply at  $\rho_2$ , see Figure 3.2b. The ALWR model uses the same supply function as the LWR model in this case. Therefore, we have

$$\min\{S^{\text{LWR}}(\rho_2), S^{\text{ARZ}}(\rho_1, \rho_2)\} = S^{\text{LWR}}(\rho_2).$$

A COMBINED FIRST AND SECOND ORDER MODEL

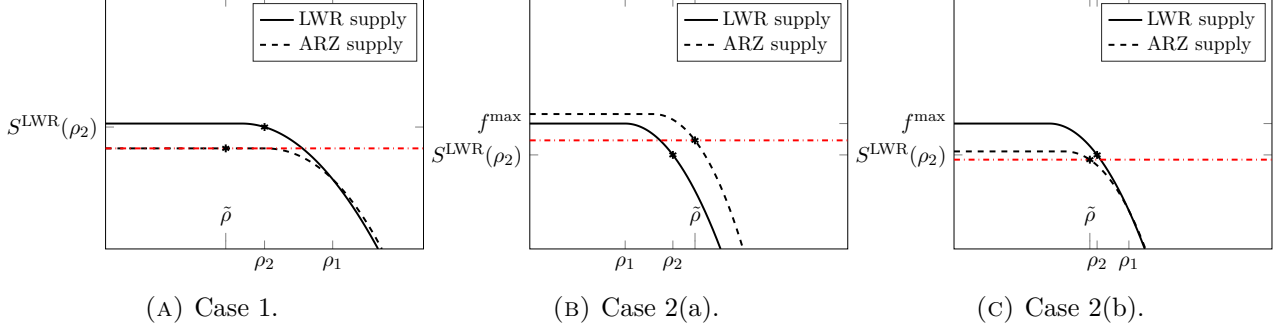


FIGURE 3.2. Supply functions  $S^{\text{LWR}}(\cdot), S^{\text{ARZ}}(\rho_1, \cdot)$ . The red line marks the value of  $S^{\text{ARZ}}(\rho_1, \rho_2)$ .

(b). The contrary is true and we have

$$\min\{S^{\text{LWR}}(\rho_2), S^{\text{ARZ}}(\rho_1, \rho_2)\} = S^{\text{ARZ}}(\rho_1, \rho_2).$$

The ALWR model therefore uses the supply function of the ARZ model, see Figure 3.2c.

TABLE 3.1. Classification of the supply function.

				Supply	Area		
$\mathcal{Z} > f^{\max}$	$\rho_1 > \rho_{\text{lim}}$	$\rho_2 \leq \rho^{\max}/2$			ARZ	I	
		$\rho_2 < \sigma_1$	$S^{\text{ARZ}}(\rho_1, 0) \geq S^{\text{LWR}}(\rho_2)$		LWR	II	
			$S^{\text{ARZ}}(\rho_1, 0) < S^{\text{LWR}}(\rho_2)$		ARZ	III	
		$\rho_2 \geq \sigma_1$	$\rho_1 \leq \rho_2$			LWR	IV
			$\rho_1 > \rho_2$	$S^{\text{ARZ}}(\rho_1, 0) \geq S^{\text{LWR}}(\rho_2)$		ARZ	V
				$S^{\text{ARZ}}(\rho_1, 0) < S^{\text{LWR}}(\rho_2)$		ARZ	VI
	$\rho_1 \leq \rho_{\text{lim}}$			LWR	VII		

Based on the previous discussion of the augmented supply function, we investigate whether the ARZ supply or the LWR supply is lower for different combinations of initial states  $(\rho_1, \rho_2) \in [0, \rho^{\max}]^2$ . The summarized cases presented in Table 3.1 lead to a partitioning of the  $\rho_1$ - $\rho_2$ -plane, which is shown in Figure 3.3. Note that the figure is only valid for  $\mathcal{Z} = D^{\text{or}} + D^{\text{LWR}}(\rho_1) > f^{\max}$ . The ARZ supply is applied in the areas I, III, V and VI while the LWR supply is applied in the areas II, IV and VII.

In the following, we prove this partitioning. Let us start with some notation to ease computations. We denote the maximum of the flux curve associated with the density  $\rho_1$  by

$$\sigma_1 = \sigma(w_1) \stackrel{(2.12)}{=} \rho^{\max} \sqrt{\frac{2w_1}{3v^{\max}}}. \quad (3.6)$$

We have that

$$\sigma(w(\rho^{\max})) = \sqrt{\frac{1}{3}}\rho^{\max} \leq \sigma_1 \leq \sigma(w(0)) = \sqrt{\frac{2}{3}}\rho^{\max}.$$

Plugging the density dependence of  $w_1$  given by (3.2) in (3.6), we denote the curve of maxima

$$\mathcal{M}(\rho_1) \stackrel{(3.2)}{=} \rho^{\max} \sqrt{\frac{1}{3} \left( \frac{\rho^{\max} - \rho_1}{\rho^{\max}} \right)^2 + \frac{1}{3}}. \quad (3.7)$$

Therefore, the curve  $\mathcal{M}(\rho_1)$  gives an expression for the curve of maxima which is decreasing in  $\rho_1$ . The maximum of the derived supply function  $S^{\text{ARZ}}(\rho_1, \cdot)$  is

$$S^{\text{ARZ}}(\rho_1, 0) = \max_{\rho_2 \in [0, \rho^{\max}]} S^{\text{ARZ}}(\rho_1, \rho_2) = \sigma_1(w_1 - p(\sigma_1)) = \rho^{\max} \left( \frac{2w_1}{3v^{\max}} \right)^{\frac{1}{2}} \frac{2}{3} w_1, \quad (3.8)$$

since for  $\rho_2 = 0$ , it follows that  $\tilde{\rho} = 0$ . From (3.2), we directly compute the density corresponding to a given  $w$ -value

$$\frac{\rho_1}{\rho^{\max}} = 1 - \sqrt{2 \frac{w_1}{v^{\max}} - 1}. \quad (3.9)$$

Then, setting

$$S^{\text{ARZ}}(\rho_{\text{lim}}, 0) = f^{\max} = \frac{\rho^{\max} v^{\max}}{4},$$

and using equation (3.8) on the left hand side, we can compute  $w_{\text{lim}}$  and the associated density  $\rho_{\text{lim}}$

$$w_{\text{lim}} = \frac{3}{2} v^{\max} \left( \frac{1}{4} \right)^{\frac{2}{3}}, \quad \frac{\rho_{\text{lim}}}{\rho^{\max}} = 1 - \sqrt{3 \left( \frac{1}{4} \right)^{\frac{2}{3}} - 1}. \quad (3.10)$$

Exemplarily, we briefly discuss case III in Table 3.1 and the corresponding region in Figure 3.3. All other cases are explained in the Appendix. Let  $\rho_1$  and  $\rho_2$  be given with

$$\rho_1 > \rho_{\text{lim}}, \quad \rho_2 > \frac{\rho^{\max}}{2}, \quad \rho_2 < \sigma_1, \quad S^{\text{ARZ}}(\rho_1, 0) < S^{\text{LWR}}(\rho_2).$$

With (3.7), the condition  $\rho_2 < \sigma_1$  is equivalent to

$$\rho_2 < \mathcal{M}(\rho_1). \quad (3.11)$$

Next, we make use of  $\rho_1 > \rho_{\text{lim}}$ ,  $\rho_2 > \frac{\rho^{\max}}{2}$  and analyze the condition

$$S^{\text{ARZ}}(\rho_1, 0) < S^{\text{LWR}}(\rho_2). \quad (3.12)$$

Applying (3.8) on the left-hand side and inserting  $S^{\text{LWR}}(\rho_2) = f(\rho_2)$  on the right-hand side yields a bound on  $\rho_2$

$$\rho_2 < \rho^{\max} \left( \frac{1}{2} + \sqrt{\frac{1}{4} - \left( \frac{1}{3} \left( \frac{\rho^{\max} - \rho_1}{\rho^{\max}} \right)^2 + \frac{1}{3} \right)^{\frac{3}{2}}} \right) := \mathcal{W}(\rho_1). \quad (3.13)$$

The area for admissible values of  $\rho_1$  and  $\rho_2$  is marked as III in Figure 3.3. Since we have  $S^{\text{ARZ}}(\rho_1, 0) < S^{\text{LWR}}(\rho_2)$ , the ARZ model is applied.

## 4. Numerical schemes and computational results

Having presented a discussion of initial states, we introduce the numerical schemes to compute solutions to the first and second order models.

### 4.1. Numerical scheme for the LWR and the combined model

We use the Godunov scheme to approximate the densities on the roads for the setting in Figure 2.1, see [19]. We consider the time horizon  $[0, T]$  and introduce a grid in time and space with step sizes  $\Delta t$ ,  $\Delta x$ . In the numerical examples, we set  $\Delta t v^{\max} \leq \Delta x$ . We denote the number of time discretizations by  $T = N_t \Delta t$ ,  $N_t \in \mathbb{N}$  and the number of spatial discretizations  $N_{x_e} \in \mathbb{N}$  on road  $e \in \mathcal{E}$  with  $L_e = N_{x_e} \Delta x$ .

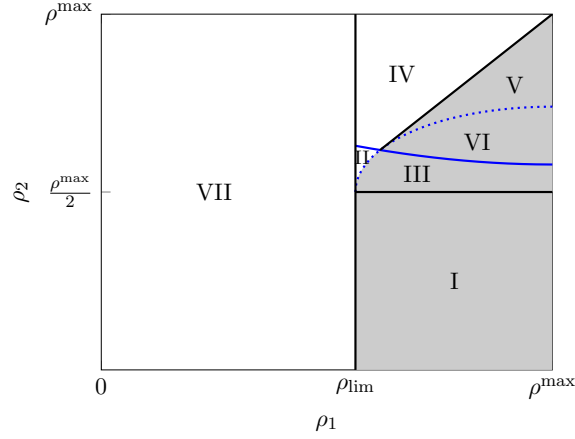


FIGURE 3.3. Partitioning of the  $\rho_1$ - $\rho_2$ -plane. Areas for the LWR supply are in white and areas for the ARZ supply are in gray. The curves  $\mathcal{M}$  (3.7) and  $\mathcal{W}$  (3.13) for  $\rho_1 \geq \rho_{\text{lim}}$  are displayed in blue (solid and dotted).

Each road is discretized with cells  $C_{e,j} = (x_{e,j-1/2}, x_{e,j+1/2})$ ,  $j = 1, \dots, N_{x_e}$ . The discretized density values  $\rho_{e,j}^s$ ,  $s = 0, \dots, N_t$  are the cell averages

$$\rho_{e,j}^s \approx \frac{1}{\Delta x} \int_{C_{e,j}} \rho_e(x, t^s) dx.$$

The Godunov scheme reads

$$\begin{aligned} \rho_{e,1}^{s+1} &= \rho_{e,1}^s - \frac{\Delta t}{\Delta x} \left( \mathcal{G}(\rho_{e,1}^s, \rho_{e,2}^s) - q_{e,in}^s \right), \\ \rho_{e,j}^{s+1} &= \rho_{e,j}^s - \frac{\Delta t}{\Delta x} \left( \mathcal{G}(\rho_{e,j}^s, \rho_{e,j+1}^s) - \mathcal{G}(\rho_{e,j-1}^s, \rho_{e,j}^s) \right), \quad j = 2, \dots, N_{x_e} - 1, \\ \rho_{e,N_{x_e}}^{s+1} &= \rho_{e,N_{x_e}}^s - \frac{\Delta t}{\Delta x} \left( q_{e,out}^s - \mathcal{G}(\rho_{e,N_{x_e}-1}^s, \rho_{e,N_{x_e}}^s) \right), \end{aligned} \quad (4.1)$$

where the Godunov flux is given by the minimum of supply and demand

$$\mathcal{G}(\rho_{e,j}^s, \rho_{e,j+1}^s) = \min\{D^{\text{LWR}}(\rho_{e,j}^s), S^{\text{LWR}}(\rho_{e,j+1}^s)\}.$$

We note that the above Godunov scheme for the computation of the density values  $\rho_{e,2}^s, \dots, \rho_{e,N_{x_e}-1}^s$  is equivalent to the cell transmission method (CTM), see [11, 15]. The inflow  $q_{e,in}^s \geq 0$  and outflow  $q_{e,out}^s \geq 0$  in (4.1) are mass fluxes at road interfaces and are determined with coupling and boundary conditions described below.

#### 1-to-1 junction with onramp

We consider a 1-to-1 junction with an additional onramp as shown in Figure 2.1. We denote the incoming road with index 1 and the outgoing road with index 2. As in [19], we assume that the demand of the onramp can be controlled and apply the demand function

$$D^{\text{or}}(l^s, t^s) = u(t^s) \min\left\{ f_{\text{or}}^{\text{in}}(t^s) + \frac{l^s}{\Delta t}, f_{\text{or}}^{\text{max}} \right\}, \quad (4.2)$$

for the onramp. Here,  $u(t) \in [0, 1]$  denotes a time-dependent metering rate which can be used to control the flow from the onramp. Moreover,  $f_{\text{or}}^{\text{max}}$  is the maximum flux allowed to enter the outgoing

road from the onramp. To define a unique solution, we assign priority parameters  $\beta$  and  $(1 - \beta)$  to road  $e = 1$  and the onramp, respectively as shown in Figure 2.1, and compute

$$q_{1,out}^s = \min\left\{D_1^{\text{LWR}}(\rho_{1,N_{x_1}}^s), \max\left\{\beta S^{\text{ALWR}}, S^{\text{ALWR}} - D^{\text{or}}(l^s, t^s)\right\}\right\}, \quad (4.3a)$$

$$q_{\text{or}}^s = \min\left\{D^{\text{or}}(l^s, t^s), \max\left\{(1 - \beta)S^{\text{ALWR}}, S^{\text{ALWR}} - D^{\text{LWR}}(\rho_{1,N_{x_1}}^s)\right\}\right\}, \quad (4.3b)$$

$$q_{2,in}^s = q_{1,out}^s + q_{\text{or}}^s, \quad (4.3c)$$

where  $S^{\text{ALWR}} = S^{\text{ALWR}}(\rho_{1,N_{x_1}}^s, \rho_{2,1}^s, l^s)$  using (2.16) and (3.4) to evaluate the ALWR supply (3.1). Similarly to the computation of the mass flux in a 2CTM for the second order model, which will be studied in Section 4.3.1, the computation of the mass fluxes  $q_{1,out}^s$ ,  $q_{\text{or}}^s$  and  $q_{2,in}^s$  considers the  $w$ -value of the incoming road  $e = 1$  in the supply function. This value of the mass flux is then used as input for the boundary cells. Especially important is that the  $w$ -value of the incoming road is derived from the density. Therefore, not the whole second order dynamics have to be tracked. We compute first order with the CTM approach and derive the second order property  $w$  from the density.

Based on the computed fluxes, the evolution of the queue at the onramp reads

$$l^{s+1} = l^s + \Delta t \left( f_{\text{or}}^{\text{in}}(t^s) - q_{\text{or}}^s \right).$$

In general, we start with empty queues, i.e.,  $l^0 = 0$ .

#### *Onramp at origin*

Additionally, we have to provide boundary data for the inflow at the beginning of the incoming road  $e = 1$ . We consider an onramp at a junction with only one outgoing road, where we denote the outgoing road with the index 1. The demand function of the onramp is given by

$$D^{\text{or}}(l^s, t^s) = \begin{cases} f_{\text{or}}^{\text{max}} & \text{if } l(t^s) > 0, \\ \min\{f_{\text{or}}^{\text{in}}(t^s) + \frac{l^s}{\Delta t}, f_{\text{or}}^{\text{max}}\} & \text{otherwise,} \end{cases} \quad (4.4)$$

where  $f_{\text{or}}^{\text{in}}(t^s)$  is the flow of cars arriving at the onramp at time  $t^s$  and  $f_{\text{or}}^{\text{max}}$  the maximum flux allowed to exit the onramp. The inflow into the system is given by

$$q_{1,in}^s = \min\{D^{\text{LWR}}(\rho_{1,1}^s), D^{\text{or}}(l^s, t^s)\}.$$

Based on the computed inflow, the evolution of the queue at the onramp is given by

$$l^{s+1} = l^s + \Delta t \left( f_{\text{or}}^{\text{in}}(t^s) - q_{1,in}^s \right).$$

#### *Junction with outflow*

At a junction with only one incoming road (denoted by index 1) and without an outgoing road, we consider absorbing boundary conditions

$$q_{1,out}^s = \min\{D^{\text{LWR}}(\rho_{1,N_{x_1}}^s), S^{\text{LWR}}(\rho_{1,N_{x_1}}^s)\}.$$

**Remark 4.1.** In comparison to the LWR onramp model in [19], only the supply function  $S^{\text{ALWR}}$  on the outgoing road of the 1-to-1 junction with onramp has been adapted in the augmented model. Therefore, replacing  $S^{\text{ALWR}}$  by  $S^{\text{LWR}}(\rho_{2,1}^s)$  in (4.3) gives the numerical discretization of the LWR model.

### 4.2. Capacity drop in comparison to the LWR model

In this section, we consider the evolution of the left- and right-hand state  $\rho_1$  and  $\rho_2$  for the Riemann problem (2.4) at the 1-to-1 junction with onramp, cf. Figure 2.1, within the ALWR model. To ensure the activation condition for the minimum in the supply function (3.1), we set  $f_{\text{or}}^{\text{in}}(t) = f_{\text{or}}^{\text{max}} = f^{\text{max}}$ . For the particular setting, solutions of Riemann problems are discussed and phase space trajectories are compared to the LWR model.

We obtain the numerical solution of the ALWR model with the scheme described in Section 4.1. The only difference to the LWR network approach presented in [19] is the modelling of the supply at the junction of the network, where we impose second-order-like conditions in the supply function, cf. Section 3. The numerical solution of the LWR model is obtained as explained in Remark 4.1. In comparison to the LWR model and as extension of the analysis in Section 3.3, the most exciting point in the ALWR model here is that the evolution of the states at the junction may lead to a change in the “active” model.

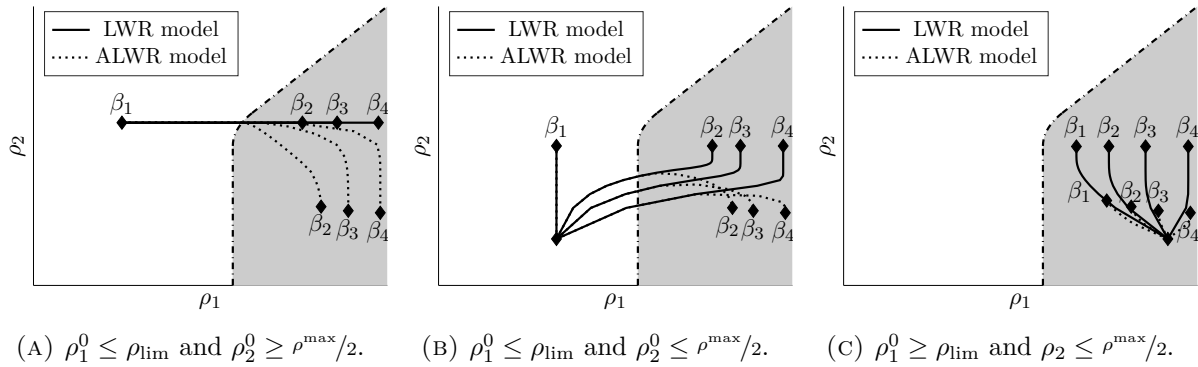


FIGURE 4.1. Comparison of the LWR and ALWR model with priority parameters  $\beta_1 = 0.9$ ,  $\beta_2 = 0.75$ ,  $\beta_3 = 0.5$  and  $\beta_4 = 0.1$ .

Due to the construction of the augmented supply function within the ALWR model as minimum of the supply functions of the LWR and the ARZ model, the solution to the Riemann problem in the ALWR model is restricted by the solution in the LWR model in the sense that the (final) supply of the outgoing road is at most as large as for the same Riemann problem in the LWR model. This means that for  $\rho_2^0 \in [0, \rho^{\text{max}}/2]$ , the arising densities on the outgoing road can never exceed  $\rho^{\text{max}}/2$ . Analogously, for  $\rho_2^0 \in [\rho^{\text{max}}/2, \rho^{\text{max}}]$ , the density on the outgoing road can never exceed  $\rho_2^0$ . We obtain weak entropy solutions on the incoming and outgoing road, see (2.5). When the current densities at the left-hand and right-hand side of the junction are in a region where the LWR supply is applied, the solution is identical to the LWR model. But as soon as the combination of the density values is in the region where the ARZ supply is applied, the supply drops below the LWR supply and the models differ.

Figure 4.1a shows the phase space trajectory for a Riemann problem with  $\rho_1^0 \in [0, \rho_{\text{lim}}]$  and  $\rho_2^0 \in [\rho^{\text{max}}/2, \rho^{\text{max}}]$  in the LWR and the ALWR model. Different priority parameters  $\beta$  are applied at the onramp. For the choice of the priority parameter  $\beta = \beta_1$ , there is no restriction on the incoming road and the density at the outgoing road remains constant. Decreasing priority parameters of the first road at some point lead to congestion at the end of the first road (as it is the case for  $\beta \in \{\beta_2, \beta_3, \beta_4\}$ ). When the phase path enters the region where the ARZ supply is applied, the phase paths of the two models diverge. In the LWR model, only the density at the incoming road increases further. In contrast, in the ALWR model, there is a drop in the density at the outgoing road due to the congestion at the end of the incoming road. The markers at the end of each trajectory indicate the final states that are reached in the respective models for the respective priority parameters.



Figure 4.1b shows the phase space trajectory for a Riemann problem with  $\rho_2^0 \in [0, \rho^{\max}/2]$ . The density on the outgoing road increases up to  $\rho^{\max}/2$  in the LWR model (since the accumulated demand is above  $f^{\max}$ ). In the ALWR model we see a different behavior. The density at the outgoing road increases at the beginning, but starts to drop down within the region where the ARZ supply is applied. Figure 4.1c exemplarily shows some trajectories with initial data in the region where the ARZ supply is applied. The fluxes in the final situation for the examples considered before are given in Table 4.1. A capacity drop in the solution for the ALWR model can be seen in all of the cases where the model differs from the LWR model. Note that here, the final fluxes  $f_2(0, T)$  at the junction match for  $\beta_2, \beta_3, \beta_4$  since the examples share the same priority parameters as well as the desired inflow from the onramp.

TABLE 4.1. Outflow  $f_2(0, T)$  in the final state at the junction with onramp (flux values in relation to  $f^{\max}$ ).

Priority Parameter	Figure 4.1a		Figure 4.1b		Figure 4.1c	
	LWR	ALWR	LWR	ALWR	LWR	ALWR
$\beta_1 = 0.90$	0.97	0.97	1	1	1	0.84
$\beta_2 = 0.75$	0.97	0.81	1	0.81	1	0.81
$\beta_3 = 0.50$	0.97	0.78	1	0.78	1	0.78
$\beta_4 = 0.10$	0.97	0.77	1	0.77	1	0.77

### 4.3. Comparison to second order models

#### 4.3.1. Numerical scheme for the ARZ and the Greenberg model

Within the ARZ and the Greenberg model, the traffic state  $U_e = (\rho_e, \rho_e w_e)$ , consisting of the density  $\rho_e$  and the generalized momentum  $\rho_e w_e$ , is computed on each road. Let  $Q_{e,j}^s$  denote the average value of the function  $U_e(x, t)$  on the interval  $C_{e,j}$  at time  $t^s = s\Delta t$ , i.e.,

$$Q_{e,j}^s = \frac{1}{\Delta x} \int_{C_{e,j}} U_{e,j}(x, t^s) dx,$$

As in [20], we apply a Godunov scheme for the flux term and an implicit Euler scheme for the relaxation term. I.e.,

$$\begin{aligned} Q_{e,1}^{s+1} &= Q_{e,1}^s - \frac{\Delta t}{\Delta x} \left( \mathcal{G}(Q_{e,1}^s, Q_{e,2}^s) - \begin{pmatrix} q_{e,in}^s \\ r_{e,in}^s \end{pmatrix} \right) + \Delta t g(Q_{e,1}^{s+1}), \\ Q_{e,j}^{s+1} &= Q_{e,j}^s - \frac{\Delta t}{\Delta x} \left( \mathcal{G}(Q_{e,j}^s, Q_{e,j+1}^s) - \mathcal{G}(Q_{e,j-1}^s, Q_{e,j}^s) \right) + \Delta t g(Q_{e,j}^{s+1}), \quad j = 2, \dots, N_{x_e} - 1, \\ Q_{e,N_{x_e}}^{s+1} &= Q_{e,N_{x_e}}^s - \frac{\Delta t}{\Delta x} \left( \begin{pmatrix} q_{e,out}^s \\ r_{e,out}^s \end{pmatrix} - \mathcal{G}(Q_{e,N_{x_e}-1}^s, Q_{e,N_{x_e}}^s) \right) + \Delta t g(Q_{e,N_{x_e}}^{s+1}), \end{aligned} \tag{4.5}$$

where there is no relaxation term for the ARZ model and for the Greenberg model, we set  $g(Q_{e,j}^s) = (0, -\rho_{e,j}^s (v_{e,j}^s - V(\rho_{e,j}^s))/\tau)^T$  equal to the right-hand side of the relaxed system (2.18). The vectors  $(q_{e,in}^s, r_{e,in}^s)^T$  and  $(q_{e,out}^s, r_{e,out}^s)^T$  in (4.5) denote mass and momentum flux at the road interfaces. The Godunov flux for the second order system formulated with the ARZ demand and supply functions (2.14)–(2.15) is given by

$$\mathcal{G}(Q_{e,j}^s, Q_{e,j+1}^s) = \begin{pmatrix} 1 \\ w_{e,j}^s \end{pmatrix} \min\{D^{\text{ARZ}}(\rho_{e,j}^s, w_{e,j}^s), S^{\text{ARZ}}(\tilde{\rho}_{e,j+1}^s, w_{e,j}^s)\},$$

where the intermediate state  $\tilde{Q}_{e,j+1}^s = (\tilde{\rho}_{e,j+1}^s, \tilde{p}_{e,j+1}^s w_{e,j}^s)^T$  used to evaluate the supply is such that

$$\tilde{\rho}_{e,j+1}^s = p^{-1} \left( \max\{w_{e,j}^s - v_{e,j+1}^s, 0\} \right).$$

In the following, we explain how the flux terms for the inflow and the outflow are given by coupling and boundary conditions.

*Onramp at origin*

We model a junction with an onramp at the beginning of the network similar as in the first order model. For the onramp with queue length  $l^s$  at time  $t^s$ , we use the demand function (4.4) to determine the mass flow  $q_{1,in}^s$ . However, due to the second order system, we have to provide also boundary data for the momentum flow. We follow the idea introduced by [20] to compute the  $w$ -value at the boundary. We compute

$$\rho_-^s = \frac{\rho^{\max}}{2} - \sqrt{\left(\frac{\rho^{\max}}{2}\right)^2 - \frac{\rho^{\max} D^{\text{or}}(l^s, t^s)}{v^{\max}}}.$$

Let  $w_-^s = w(\rho_-^s) = V(\rho_-^s) + p(\rho_-^s)$ , then we can model the boundary fluxes by

$$\begin{pmatrix} q_{1,in}^s \\ r_{1,in}^s \end{pmatrix} = \begin{pmatrix} 1 \\ w_-^s \end{pmatrix} \min\{D^{\text{or}}(l^s, t^s), S^{\text{ARZ}}(\tilde{\rho}_{1,0}^s, w_-^s)\},$$

with  $\tilde{\rho}_{1,0}^s = p^{-1} \left( \max\{w_-^s - v_{1,1}^s, 0\} \right)$ .

*1-to-1 junction with onramp*

At the 1-to-1 junction with onramp, we denote the incoming road  $e = 1$  and outgoing road  $e = 2$ . We assume that the onramp can be controlled by the time-dependent metering rate  $u(t)$  and compute the controlled onramp demand with equation (4.2). The fluxes at the road interfaces are given by

$$\begin{aligned} \begin{pmatrix} q_{1,out}^s \\ r_{1,out}^s \end{pmatrix} &= \begin{pmatrix} 1 \\ w_{1,N_{x_1}}^s \end{pmatrix} \min\left\{D_1, \max\{\beta S_2, S_2 - D^{\text{or}}(l^s, t^s)\}\right\}, \\ \begin{pmatrix} q_{\text{or},out}^s \\ r_{\text{or},out}^s \end{pmatrix} &= \begin{pmatrix} 1 \\ w_{1,N_{x_1}}^s \end{pmatrix} \min\left\{D^{\text{or}}(l^s, t^s), \max\{(1 - \beta)S_2, S_2 - D_1\}\right\}, \\ \begin{pmatrix} q_{2,in} \\ r_{2,in} \end{pmatrix} &= \begin{pmatrix} 1 \\ w_{1,N_{x_1}}^s \end{pmatrix} (q_{1,out}^s + q_{\text{or},out}^s), \end{aligned}$$

where

$$D_1 = D^{\text{ARZ}}(\rho_{1,N_{x_1}}^s, w_{1,N_{x_1}}^s), \quad S_2 = S^{\text{ARZ}}(\tilde{\rho}_{2,1}^s, w_{1,N_{x_1}}^s), \quad \tilde{\rho}_{2,1}^s = p^{-1} \left( \max\{w_{1,N_{x_1}}^s - v_{2,1}^s, 0\} \right)$$

*Junction with outflow*

At a junction with only one incoming road (denoted by index 1), we consider absorbing boundary conditions. We have

$$\begin{pmatrix} q_{1,out}^s \\ r_{1,out}^s \end{pmatrix} = \begin{pmatrix} 1 \\ w_{N_{x_1}-1}^s \end{pmatrix} \min\left\{D^{\text{ARZ}}\left(\rho_{N_{x_1}-1}^s, w_{N_{x_1}-1}^s\right), S^{\text{ARZ}}\left(\rho_{N_{x_1}-1}^s, w_{N_{x_1}-1}^s\right)\right\}.$$

Analogously to Godunov scheme for the first order models, the Godunov approximation for the second order models is mathematically equivalent to a cell transmission model (2CTM), see [15], using the supply function of the ARZ model and the two quantities  $\rho, w$ .

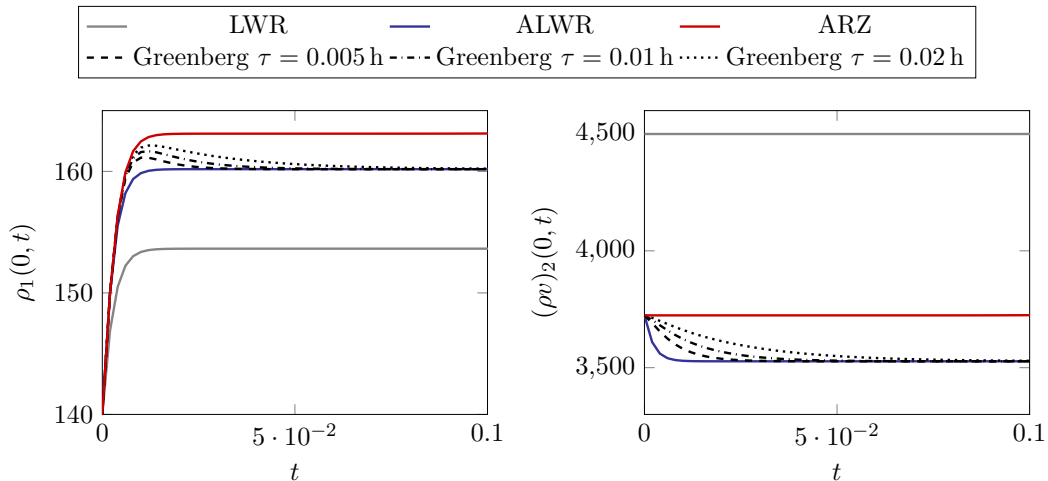
4.3.2. Capacity drop in comparison to second order models

We consider the network depicted in Figure 2.1 with the parameters given in Table 4.2, which are inspired by the onramp scenario in [20, Section 4.3]. We set  $\Delta x = 0.25$  km,  $\Delta t = 2 \cdot 10^{-3}$  h and the desired inflow from the onramp to  $f_{or}^{in} = 4000 \frac{\text{cars}}{\text{h}}$  and the maximum flux allowed to exit the onramp equal to the maximum flux of the outgoing road  $f_{or}^{max} = 4500 \frac{\text{cars}}{\text{h}}$ . The priority is  $\beta = 0.5$  and the incoming road therefore experiences congestion. We compute the time evolution of the (half-) Riemann problem (2.4) with  $\rho_1^0 = 140$ ,  $\rho_2^0 = 90$  within the LWR and ALWR model. Within the ARZ and the Greenberg model, we compute the time evolution of the (half-) Riemann problem (2.13) with initial states  $(\rho_1^0, w_1^0)$ ,  $(\rho_2^0, w_2^0)$  where  $w_e^0 = V(\rho_e^0) + p(\rho_e^0)$ ,  $e = 1, 2$ .

The density at the end of the incoming road increases in all models, see Figure 4.2a. The density in the Greenberg model increases similar to the ARZ model but is relaxed towards the ALWR flux as time progresses. The discharge flow of the junction in the LWR model stays at the level of the maximum flow even as further congestion on the incoming road sets on, compare Figure 4.2b. In contrast, all of the other models predict a decrease in the discharge flow at the junction. At  $t = 0$ , the flux  $(\rho v)_2(0, 0)$  is identical for the Greenberg and the ARZ model. However, the flux in the Greenberg model is relaxed until a state on the LWR fundamental diagram is reached. The ALWR model mimics the flux of the second order model at the junction. We see a capacity drop since the discharge flow is lower than the maximum flux due to congestion on the incoming road. The behavior observed in Figure 4.2 stays the same, also for varying parameters  $\gamma > 1$  for which the fluxes through the junction for the respective models are given in Table 4.3. The flux in the Greenberg model at  $t = 0$  is identical to the flux in the ARZ model and afterwards drops down to the level of the ALWR flux at  $T = 0.1$

TABLE 4.2. Properties of the roads in Figure 2.1.

road	length [km]	$\rho^{\max} [\frac{\text{cars}}{\text{km}}]$	$v^{\max} [\frac{\text{km}}{\text{h}}]$	initial density $\rho^0 [\frac{\text{cars}}{\text{km}}]$
road 1	4	180	100	140
road 2	2	180	100	90



(A) Density at the end of the incoming road. (B) Mass flux into the outgoing road.

FIGURE 4.2. Densities and fluxes.

TABLE 4.3. Fluxes of the Riemann problem for different values of  $\gamma$  with  $T = 0.1$ .

$\gamma$	$w_1$	$w_2$	ARZ $(\rho v)_2(0, T)$	ALWR $(\rho V)_2(0, T)$
1.0	100	100	4500.00	4500.00
1.5	67.95	73.57	4035.68	3948.09
2.0	52.47	62.50	3724.53	3527.28
2.5	43.56	57.07	3511.85	3194.02
3.0	37.91	54.17	3365.52	2922.56

4.3.3. *The ramp metering control problem*

We consider an onramp with ramp metering as introduced in Section 4.1 and 4.3.1 with a piecewise constant control function  $u(t)$  on intervals of 15 minutes. Our aim is to compare the optimal control of the ALWR model with optimal control results of the Greenberg model. We consider the relaxation time  $\tau = 0.005$  h for the Greenberg model (2.18) and the parameters from Table 4.2 but set the initial densities to  $\rho_e^0 = 50 \frac{\text{cars}}{\text{km}}$ ,  $e = 1, 2$  such that both roads have equal traffic volume at  $t = 0$ . The priority parameter  $\beta$  at the onramp equals 0.5 and we set the maximum inflow from the onramp to  $f_{\text{or}}^{\text{max}} = 2000 \frac{\text{cars}}{\text{h}}$ . Additionally, we consider an onramp at the origin *in* with  $f_{\text{or}}^{\text{max}} = 4500 \frac{\text{cars}}{\text{h}}$ . The time horizon is  $T = 3$  hours. The applied discretization parameters are  $\Delta x = 0.25$  km and  $\Delta t = 2 \cdot 10^{-3}$  h and we apply the discretization schemes described in Section 4.1 and 4.3.1.

For the control scenario, we apply the inflow conditions shown in Figure 4.3a. At the beginning of the time horizon, we consider a first rush-hour with moderate demand at the onramp. Later on, we consider a second rush-hour, with increased onramp demand. For the given scenario, we are interested in minimizing the total travel time

$$\sum_{e=1}^2 \int_0^T \int_0^{L_e} \rho_e(x, t) dx dt + \sum_{e=1}^2 \int_0^T l_e(t) dt, \tag{4.6}$$

where  $l_1$  denotes the queue at *in* and  $l_2$  the queue at *ramp*. To solve this optimization task, we apply a first-discretize-then-optimize approach. Thus, for given control decisions (time-dependent piecewise constant metering rates), the discretization schemes are always used to evaluate the objective function (4.6) and iteratively compute optimal solutions. The Matlab solver *fmincon*<sup>2</sup> is used for the optimization of the control decisions. Having the optimal control of the ALWR model at hand, we use this control as a starting value for the optimization in the Greenberg model.

TABLE 4.4. Optimization results (total travel time [h]) for the network in Figure 2.1.

	Greenberg	ALWR	LWR
no control	1236.5	1316.0	1019.3
optimal control ALWR	996.6	1019.6	1019.6
optimal control Greenberg	982.3	1322.9	1019.5

Table 4.4 shows the total travel times for the different models with and without optimization ( $u(t) = 1 \forall t$ ). The resulting queues are shown in Figure 4.4, where we show the Greenberg model to demonstrate the benefit of the optimized control computed with the cheaper ALWR model.

Running a simulation with the Greenberg model using the optimal control of the ALWR model leads to a total travel time of 996.6, which is about 1.5% away from the optimal solution found by

<sup>2</sup><https://de.mathworks.com/help/optim/ug/fmincon.html>

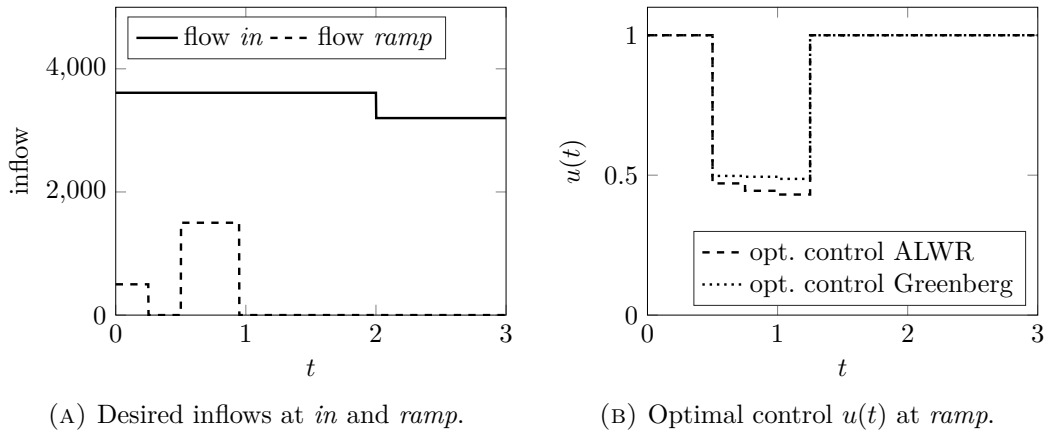


FIGURE 4.3. Inflow and controls.

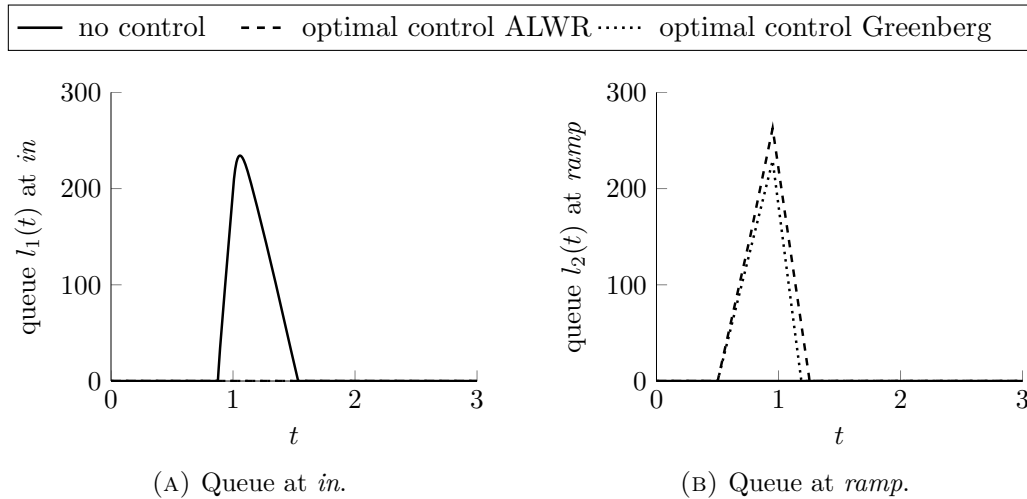


FIGURE 4.4. Queues in the Greenberg model with and without optimization.

optimizing the Greenberg model, see Table 4.4. Actually, the optimal metering rates for the two models do not differ much, see Figure 4.3b. The key in improving the travel times is the reduction of the flow from the onramp in the time frame of high onramp demand, compare Figure 4.3. Both controls do not reduce the onramp demand during the first rush-hour, but reduce it during the second rush-hour to ensure that the incoming road stays in free flow. Without control, the queue at the onramp stays empty whereas more than 200 cars accumulate in the queue at the origin, see Figure 4.4. When the optimal control of the Greenberg or the ALWR model is used, the queue at the origin is reduced to zero, while the cars accumulate in the queue at the onramp during the rush-hour time. Ramp metering leads to an increased outflow at the end of the outgoing road early within the time horizon, see Figure 4.5. Note that an optimal control strategy cannot be recognized by an optimal control approach based on the LWR model since full inflow, i.e.,  $u(t) = 1 \forall t$  is optimal for the LWR model. However, this is clearly not optimal for the Greenberg model, see Table 4.4.

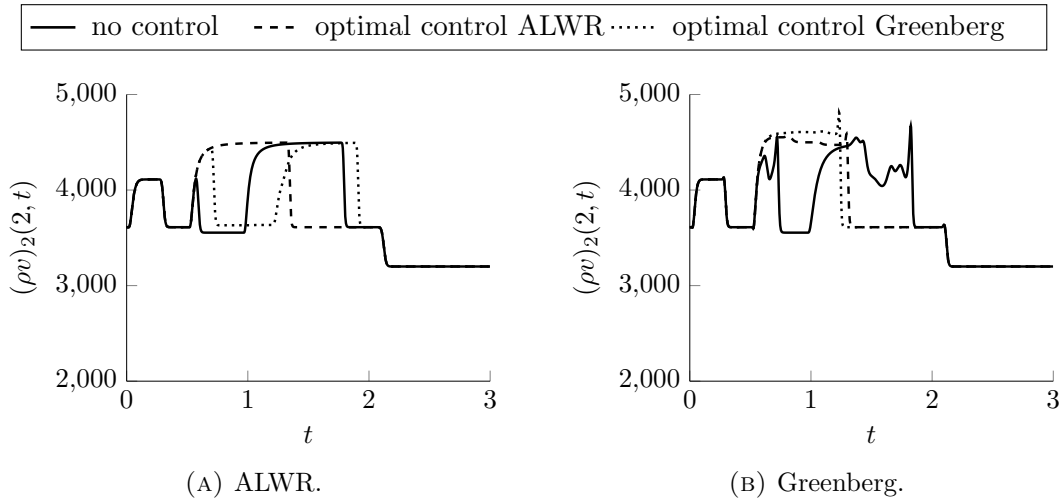


FIGURE 4.5. Flow at the end of the outgoing road *out* with and without optimization.

## 5. Conclusion

We have established a new model for the 1-to-1 junction with onramp which couples the LWR model to boundary conditions of the second order traffic model. The main difference to earlier presented versions of the LWR model is the shape of the supply function at the junction, which allows for formation of congestion when the incoming road is congested. A discussion of the new supply function was presented and we have shown that the fluxes at the junctions are only dependent on the densities of the adjacent roads. Numerical studies have shown that the ALWR model is able to capture the capacity drop phenomenon. Even though the junction model is a modification of the most simple traffic model for traffic flows, we achieved promising results and were able to capture at least some aspects of second order traffic models. Optimization results showed that the ALWR model is a suitable surrogate for the Greenberg model. In the considered scenario, the ALWR model optimum is close to the optimum of the Greenberg model. Note that similar considerations can be done analogously for exponents  $\gamma > 1$  in the pressure function which is postponed to future work.

## Appendix A.

We begin with some general observations which are useful to derive the partitioning of the  $\rho_1$ - $\rho_2$ -plane in Figure 3.3. For fixed  $\rho_1$ , the value of  $\tilde{\rho}$  given by (3.4) increases with  $\rho_2$

$$\partial_{\rho_2} \tilde{\rho} \geq 0. \tag{A.1}$$

Moreover, due to (A.1), the partial derivative for the density on the outgoing road of the derived ARZ supply (3.3) satisfies

$$\partial_{\rho_2} S^{\text{ARZ}}(\rho_1, \rho_2) \leq 0. \tag{A.2}$$

Thus, the larger  $\rho_2$ , the larger  $\tilde{\rho}$  and the lower the ARZ supply. Furthermore, for  $\rho_1 = \rho_2$ , we have  $\tilde{\rho} = \rho_1 = \rho_2$ . Now, we have a closer look at  $\tilde{\rho}$  for  $\rho_2 \geq \rho_1$ . We show that

$$\tilde{\rho} = p^{-1}(p(\rho_1) + V_1 - V_2) \geq \rho_2. \tag{A.3}$$

This is equivalent to

$$\begin{aligned} p(\rho_1) + V_1 - V_2 &\geq p(\rho_2) \\ v^{\max} \left( \frac{\rho_2 - \rho_1}{\rho^{\max}} + \frac{\rho_1^2}{2(\rho^{\max})^2} \right) &\geq \frac{v^{\max}}{2} \left( \frac{\rho_2}{\rho^{\max}} \right)^2 \\ \frac{\rho_2 - \rho_1}{\rho^{\max}} &\geq \frac{\rho_2^2 - \rho_1^2}{2(\rho^{\max})^2} \\ 2\rho^{\max} &\geq \rho_1 + \rho_2, \end{aligned}$$

which is satisfied for any combination  $(\rho_1, \rho_2) \in [0, \rho^{\max}]^2$ . In the following, we prove the partitioning of the  $\rho_1$ - $\rho_2$ -plane.

**I.** The analysis for

$$\rho_1 > \rho_{\text{lim}}, \quad \rho_2 \leq \frac{\rho^{\max}}{2},$$

is straightforward. The area of admissible combinations  $(\rho_1, \rho_2)$  is shown in area I of Figure 3.3. By the definition of  $\rho_{\text{lim}}$ , cf. equation (3.5), it holds that

$$S^{\text{LWR}}(\rho_2) = f^{\max} > S^{\text{ARZ}}(\rho_1, 0).$$

Therefore,  $S^{\text{LWR}}(\rho_2) > S^{\text{ARZ}}(\rho_1, \rho_2)$  holds and the ARZ supply is applied.

**VII.** We analyze more closely the case  $\rho_1 \leq \rho_{\text{lim}}$ , which is the area VII in Figure 3.3. By the definition of  $\rho_{\text{lim}}$ , cf. equation (3.5), we have that  $S^{\text{ARZ}}(\rho_1, 0) \geq f^{\max}$ .

(a) Assume first that  $\rho_1 \geq \rho_2$ . Then

$$\tilde{\rho} = p^{-1}(\max\{0, V_1 - V_2 + p(\rho_1)\}) \leq \rho_1 < \mathcal{M}(\rho_1),$$

and this leads to

$$S^{\text{ARZ}}(\rho_1, \rho_2) = S^{\text{ARZ}}(\rho_1, 0) \geq f^{\max} \geq S^{\text{LWR}}(\rho_2).$$

(b) Assume now  $\rho_2 > \rho_1$  and  $\rho_2 \geq \rho^{\max}/2$ .

(b1) Assume  $\tilde{\rho} \geq \sigma_1$ . Then we have

$$S^{\text{ARZ}}(\rho_1, \rho_2) = \tilde{\rho}(w_1 - (w_1 - V_2)) = \tilde{\rho}V_2 \geq \rho_2V_2 = S^{\text{LWR}}(\rho_2),$$

where we made use of the relation of  $\tilde{\rho}$  and  $\rho_2$  in equation (A.3).

(b2) If instead we have  $\tilde{\rho} < \sigma_1$ , then

$$S^{\text{ARZ}}(\rho_1, \rho_2) = S^{\text{ARZ}}(\rho_1, 0) \geq S^{\text{LWR}}(\rho_2),$$

due to the assumption  $\rho_1 \leq \rho_{\text{lim}}$ .

(c) Assume  $\rho_2 > \rho_1$  and  $\rho_2 < \rho^{\max}/2$ . From a) and b), we deduce

$$S^{\text{ARZ}} \left( \rho_1, \frac{\rho^{\max}}{2} \right) \geq f^{\max}, \quad \forall \rho_1 \in [0, \rho_{\text{lim}}].$$

Moreover since (A.2) holds true, we know that

$$S^{\text{ARZ}}(\rho_1, \rho_2) \geq f^{\max} = S^{\text{LWR}}(\rho_2), \quad \forall \rho_1 \in [0, \rho_{\text{lim}}], \rho_2 \in \left( \rho_1, \frac{\rho^{\max}}{2} \right).$$

**II.** Let  $(\rho_1, \rho_2)$  be given with

$$\rho_1 > \rho_{\text{lim}}, \quad \rho_2 > \frac{\rho^{\max}}{2}, \quad \rho_2 < \sigma_1, \quad S^{\text{ARZ}}(\rho_1, 0) \geq S^{\text{LWR}}(\rho_2).$$

Because  $\rho_2 < \sigma_1$ , we get the inequality  $\rho_2 < \mathcal{M}(\rho_1)$  from (3.11). Moreover due to  $S^{\text{ARZ}}(\rho_1, 0) \geq S^{\text{LWR}}(\rho_2)$ , compare (3.12), we know from (3.13) that  $\rho_2 \geq \mathcal{W}(\rho_1)$ . This gives the area II in the  $\rho_1$ - $\rho_2$ -plane in Figure 3.3. For given  $(\rho_1, \rho_2)$  in area II, we have to proof that the LWR model is applied. We can proceed similarly as for region VII:

For  $\rho_1 \geq \rho_2$ , it holds that  $\tilde{\rho} \leq \rho_1 \leq \mathcal{M}(\rho_1)$  and  $S^{\text{ARZ}}(\rho_1, \rho_2) = S^{\text{ARZ}}(\rho_1, 0) \geq S^{\text{LWR}}(\rho_2)$ .

For  $\rho_2 > \rho_1 \geq \rho^{\max}/2$ , we distinguish again. If  $\tilde{\rho} \geq \sigma_1$ , then  $S^{\text{ARZ}}(\rho_1, \rho_2) = \tilde{\rho}V_2 \geq \rho_2V_2$ . If instead  $\tilde{\rho} < \sigma_1$ , then  $S^{\text{ARZ}}(\rho_1, \rho_2) = S^{\text{ARZ}}(\rho_1, 0) \geq S^{\text{LWR}}(\rho_2)$ .

**IV.** Let  $(\rho_1, \rho_2)$  satisfy the assumptions

$$\rho_1 > \rho_{\text{lim}}, \quad \rho_2 > \frac{\rho^{\max}}{2}, \quad \rho_2 \geq \sigma_1, \quad \rho_1 \leq \rho_2.$$

The area for admissible values of  $\rho_1$  and  $\rho_2$  is marked in Figure 3.3 as area IV. We know from equation (A.3) and the assumption here, that  $\tilde{\rho} \geq \rho_2 \geq \sigma_1$ . Therefore,

$$S^{\text{ARZ}}(\rho_1, \rho_2) = \tilde{\rho}V_2 \geq S^{\text{LWR}}(\rho_2).$$

**V.** Let

$$\rho_1 > \rho_{\text{lim}}, \quad \rho_2 > \frac{\rho^{\max}}{2}, \quad \rho_2 \geq \sigma_1, \quad \rho_1 > \rho_2, \quad S^{\text{ARZ}}(\rho_1, 0) \geq S^{\text{LWR}}(\rho_2).$$

For the region V, it holds that  $w_1 \geq w(\rho^{\max}) = v^{\max}/2$  and  $V_2 < v^{\max}/2$ . Thus,

$$w_1 - V_2 > 0.$$

Similarly to the proof of (A.3), one can show

$$\tilde{\rho} = p^{-1}(p(\rho_1) + V_1 - V_2) \leq \rho_2. \quad (\text{A.4})$$

Moreover, we prove

$$\begin{aligned} \tilde{\rho} &> \sigma_1 \\ p^{-1}(w_1 - V_2) &> \sigma_1 \\ w_1 - V_2 &> p(\sigma_1) = \frac{w_1}{3} \\ \frac{2}{3}w_1 &> V_2 \\ \frac{2}{3} \left( v^{\max} \frac{\rho^{\max} - \rho_1}{\rho^{\max}} + \frac{v^{\max}}{2} \left( \frac{\rho_1}{\rho^{\max}} \right)^2 \right) &> v^{\max} \frac{\rho^{\max} - \rho_2}{\rho^{\max}} \\ \rho_2 &> \rho^{\max} - \frac{2}{3}(\rho^{\max} - \rho_1) - \frac{1}{3} \frac{\rho_1^2}{\rho^{\max}} =: \Sigma(\rho_1). \end{aligned} \quad (\text{A.5})$$

For  $(\rho_1, \rho_2)$  in region V, we have  $\rho_2 > \Sigma(\rho_1)$ , see Figure A.1. Therefore  $\tilde{\rho} > \sigma_1$  and, using also (A.4), we get

$$S^{\text{ARZ}}(\rho_1, \rho_2) = \tilde{\rho}V_2 \leq \rho_2V_2 = S^{\text{LWR}}(\rho_2).$$



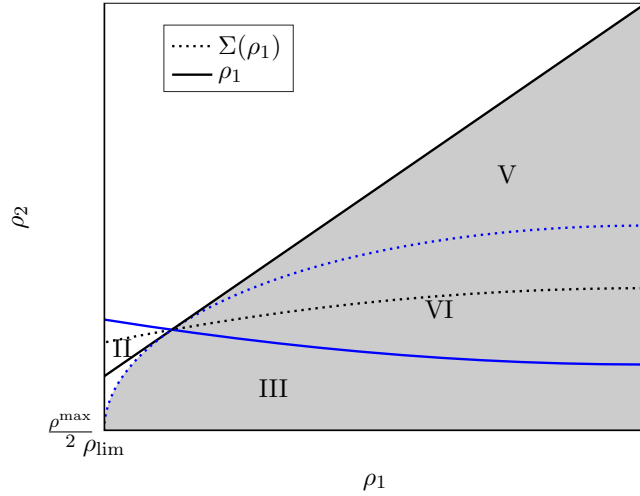


FIGURE A.1. Zoom into the regions II, III, V and VI. The curves (3.7) and (3.13) are displayed in blue (solid and dotted).

**VI.** Let

$$\rho_1 > \rho_{\text{lim}}, \quad \rho_2 > \frac{\rho^{\max}}{2}, \quad \rho_2 \geq \sigma_1, \quad \rho_1 > \rho_2, \quad S^{\text{ARZ}}(\rho_1, 0) < S^{\text{LWR}}(\rho_2).$$

Since  $S^{\text{ARZ}}(\rho_1, 0) < S^{\text{LWR}}(\rho_2)$  is claimed, the ARZ supply is applied. Now, since  $\rho_2 \geq \sigma_1$ , we get from (3.11)

$$\rho_2 \geq \mathcal{M}(\rho_1),$$

which is the area above the lower curve limiting region VI in Figure 3.3. Next, by the condition  $S^{\text{ARZ}}(\rho_1, 0) < S^{\text{LWR}}(\rho_2)$ , we know from (3.13) that

$$\rho_2 < \mathcal{W}(\rho_1),$$

which is below the upper limiting curve of region VI in Figure 3.3.

## References

- [1] Boris Andreianov, Carlotta Donadello, Ulrich Razafison, and Massimiliano D. Rosini. Riemann problems with non-local point constraints and capacity drop. *Math. Biosci. Eng.*, 12:259–278, 2015.
- [2] Boris Andreianov, Carlotta Donadello, and Massimiliano D. Rosini. A second-order model for vehicular traffics with local point constraints on the flow. *Math. Models Methods Appl. Sci.*, 26:751–802, 2016.
- [3] A. Aw, A. Klar, T. Materne, and M. Rascle. Derivation of continuum traffic flow models from microscopic follow-the-leader models. *SIAM J. Appl. Math.*, 63:259–278, 2002.
- [4] A. Aw and M. Rascle. Resurrection of “Second Order” Models of Traffic Flow. *SIAM J. Appl. Math.*, 60:916–938, 2000.
- [5] James H. Banks. Freeway bottlenecks: a basis for ramp metering? *Transportation Research Record*, 1320:83–90, 1991.
- [6] Alberto Bressan. *Hyperbolic Systems of Conservation Laws: The One-Dimensional Cauchy Problem*, volume 20. Oxford University Press, reprinted edition, 2005.
- [7] Alberto Bressan, Sunčica Čanić, Mauro Garavello, Michael Herty, and Benedetto Piccoli. Flows on networks: recent results and perspectives. *EMS Surv. Math. Sci.*, 1:47–111, 2014.

- [8] Michael J. Cassidy and Robert L. Bertini. Some traffic features at freeway bottlenecks. *Transportation Research Part B: Methodological*, 33:25–42, 1999.
- [9] Koohong Chung, Jittichai Rudjanakanoknad, and Michael J. Cassidy. Relation between traffic density and capacity drop at three freeway bottlenecks. *Transportation Research Part B: Methodological*, 41:82–95, 2007.
- [10] Giuseppe M. Coclite, Mauro Garavello, and Benedetto Piccoli. Traffic flow on a road network. *SIAM J. Math. Anal.*, 36:1862–1886, 2005.
- [11] Carlos F. Daganzo. The cell transmission model: A dynamic representation of highway traffic consistent with the hydrodynamic theory. *Transportation Research Part B: Methodological*, 28:269–287, 1994.
- [12] Carlos F. Daganzo. Requiem for second-order fluid approximations of traffic flow. *Transportation Research Part B: Methodological*, 29:277–286, 1995.
- [13] Edda Dal Santo, Carlotta Donadello, Sabrina F. Pellegrino, and Massimiliano D. Rosini. Representation of capacity drop at a road merge via point constraints in a first order traffic model. *ESAIM, Math. Model. Numer. Anal.*, 53:1–34, 2019.
- [14] Maria Laura Delle Monache, Jack Reilly, Samitha Samaranyake, Walid Krichene, Paola Goatin, and Alexandre M. Bayen. A PDE-ODE model for a junction with ramp buffer. *SIAM J. Appl. Math.*, 74:22–39, 2014.
- [15] Shimao Fan, Ye Sun, Benedetto Piccoli, Benjamin Seibold, and Daniel B. Work. A collapsed generalized Aw–Rascle–Zhang model and its model accuracy. <http://arxiv.org/abs/1702.03624>, 2017.
- [16] Mauro Garavello and Benedetto Piccoli. Traffic flow on a road network using the Aw–Rascle model. *Commun. Partial Differ. Equations*, 31:243–275, 2006.
- [17] Mauro Garavello and Benedetto Piccoli. *Traffic Flow On Networks*, volume 1 of *AIMS Series on Applied Mathematics*. American Institute of Mathematical Sciences, 2006.
- [18] Paola Goatin. The Aw–Rascle vehicular traffic flow model with phase transitions. *Math. Comput. Modelling*, 44:287–303, 2006.
- [19] Paola Goatin, Simone Göttlich, and Oliver Kolb. Speed limit and ramp meter control for traffic flow networks. *Engineering Optimization*, 48:1121–1144, 2016.
- [20] Paola Goatin, Simone Göttlich, and Oliver Kolb. Capacity drop and traffic control for a second order traffic model. *Netw. Heterog. Media*, 12:663–681, 2017.
- [21] James M. Greenberg. Extensions and amplifications of a traffic model of Aw and Rascle. *SIAM J. Appl. Math.*, 62:729–745, 2002.
- [22] Fred L. Hall and Kwaku Agyemang-Duah. Freeway capacity drop and the definition of capacity. *Transportation Research Record*, 1320:91–98, 2000.
- [23] Bertrand Haut and Georges Bastin. A second order model of road junctions in fluid models of traffic networks. *Netw. Heterog. Media*, 2:227–253, 2007.
- [24] Bertrand Haut, Georges Bastin, and Yacine Chitour. A macroscopic traffic model for road networks with a representation of the capacity drop phenomenon at the junctions. *IFAC Proceedings Volumes*, 38:114–119, 2005.
- [25] Dirk Helbing. Traffic and related self-driven many-particle systems. *Rev. Mod. Phys.*, 73:1067–1141, 2001.
- [26] M. Herty and S. Moutari. A macro-kinetic hybrid model for traffic flow on road networks. *Comput. Methods Appl. Math.*, 9:238–252, 2009.
- [27] M. Herty, S. Moutari, and M. Rascle. Optimization criteria for modelling intersections of vehicular traffic flow. *Netw. Heterog. Media*, 1:275–294, 2006.
- [28] M. Herty and M. Rascle. Coupling conditions for a class of second-order models for traffic flow. *SIAM J. Math. Anal.*, 38:595–616, 2006.

- [29] Michael Herty and Axel Klar. Modeling, simulation, and optimization of traffic flow networks. *SIAM J. Sci. Comput.*, 25:1066–1087, 2003.
- [30] Helge Holden and Nils Henrik Risebro. A mathematical model of traffic flow on a network of unidirectional roads. *SIAM J. Math. Anal.*, 26:999–1017, 1995.
- [31] Oliver Kolb, Guillaume Costeseque, Paola Goatin, and Simone Göttlich. Pareto-optimal coupling conditions for the Aw–Rascle–Zhang traffic flow model at junctions. *SIAM J. Appl. Math.*, 78:1981–2002, 2018.
- [32] Stanislav N. Kružkov. First order quasilinear equations in several independent variables. *Math. USSR, Sb.*, 10, 1970.
- [33] Peter D. Lax. *Hyperbolic Systems of Conservation Laws and the Mathematical Theory of Shock Waves*. Society for Industrial and Applied Mathematics, 1973.
- [34] J. P. Lebacque. Intersection Modeling, Application to Macroscopic Network Traffic Flow Models and Traffic Management. In *Traffic and Granular Flow '03*, pages 261–278. Springer, 2005.
- [35] Jean Patrick Lebacque. Two-phase bounded-acceleration traffic flow model: analytical solutions and applications. *Transportation Research Record*, 1852:220–230, 2003.
- [36] Michael James Lighthill and Gerald B. Whitham. On kinematic waves. II. A theory of traffic flow on long crowded roads. *Proc. R. Soc. Lond., Ser. A*, 229:317–345, 1955.
- [37] Markos Papageorgiou and Apostolos Kotsialos. Freeway ramp metering: An overview. *IEEE Transactions on Intelligent Transportation Systems*, 3:271–281, 2002.
- [38] Celine Parzani and Christine Buisson. Second-order model and capacity drop at merge. *Transportation Research Record*, 2315:25–34, 2012.
- [39] M. Rascle. An improved macroscopic model of traffic flow: derivation and links with the Lighthill-Whitham model. *Math. Comput. Modelling*, 35:581–590, 2002.
- [40] Jack Reilly, Samitha Samaranayake, Maria Laura Delle Monache, Walid Krichene, Paola Goatin, and Alexandre M. Bayen. Adjoint-based optimization on a network of discretized scalar conservation laws with applications to coordinated ramp metering. *J. Optim. Theory Appl.*, 167:733–760, 2015.
- [41] Paul I. Richards. Shock waves on the highway. *Oper. Res.*, 4:42–51, 1956.
- [42] Florian Siebel and Wolfram Mauser. On the fundamental diagram of traffic flow. *SIAM J. Appl. Math.*, 66:1150–1162, 2006.
- [43] Florian Siebel, Wolfram Mauser, Salissou Moutari, and Michel Rascle. Balanced vehicular traffic at a bottleneck. *Math. Comput. Modelling*, 49:689–702, 2009.
- [44] Martin Treiber and Arne Kesting. *Traffic Flow Dynamics: Data, Models and Simulation*. Springer, 1 edition, 2013.
- [45] H. M. Zhang. A non-equilibrium traffic model devoid of gas-like behavior. *Transportation Research Part B: Methodological*, 36:275–290, 2002.